7

Single-Molecule Studies of Rotary Molecular Motors

Teuta Pilizota, Yoshiyuki Sowa, and Richard M. Berry

Abstract Rotary molecular motors are protein complexes that transform chemical or electrochemical energy into mechanical work. There are five known rotary molecular motors in nature; the bacterial flagellar motor, and two motors in each of ATP-synthase and V-ATPase. Rotation of the flagellar motor drives a helical propeller that powers bacterial swimming. The function of the other rotary motors is to couple electrochemical ion gradients to synthesis or hydrolysis of ATP, and rotation is a detail of the coupling mechanism rather than the ultimate purpose of the motors. Much has been learned about the mechanism of the F_1 part of ATP-synthase and the flagellar motor by measuring the rotation of single motors with a variety of techniques under a wide range of conditions. This chapter will review the structures of ATP-synthase and the flagellar motor, and what has been learned about their mechanisms using single molecule techniques.

7.1. Introduction

Rotarymolecular motors are protein complexes that transform chemical or electrochemical energy into mechanical work. The work done is defined as the product of torque (force times the perpendicular distance to the axis of rotation) and the relative angle of rotation between a fixed part designated the stator and a moving part designated the rotor. There are five known rotary molecular motors in nature (we will not consider here DNA-processing motors with a rotary component to their motion). The bacterial flagellar motor (BFM), the F_o part of ATP-synthase, and the V_o part of ion-pumping V-ATPases are driven by electrochemical gradients (ion-motive forces [IMFs]) of H^+ ions (protonmotive force [PMF]) or Na^+ ions (sodium-motive force [SMF]) across energized membranes. The F_1 and V_1 parts of ATP-synthase and V-ATPases are driven by ATP hydrolysis. In the BFM, the stator is a ring of independent torque-generating units anchored to the cell wall, and the rotor is a set of rings $\sim$45 nm in diameter that spans the bacterial envelope. In ATP-synthase and V-ATPases, the stators of the F/V_o and F/V_1 parts are connected together by a peripheral stalk, and the rotors are connected together by a central stalk. The dimensions

T. Pillizota, Y. Sowa, and R. M. Berry • Department of Physics, Clarendon Lab, University of Oxford, Oxford OX1 3PU, UK

P. Hinterdorfer, A. van Oijen (eds.), *Handbook of Single-Molecule Biophysics*,
DOI 10.1007/978-0-387-76497-9_7,

of both enzymes are roughly 10 nm in diameter by 20 nm long. Whereas rotation of the BFM drives a helical propeller that powers bacterial swimming, the function of the other rotary motors is to couple the IMF to synthesis or hydrolysis of adenosine triphosphate (ATP), and rotation is a detail of the coupling mechanism rather than the ultimate purpose of the motors. Much has been learned about the mechanism of F_1 and the BFM by measuring the rotation of single motors with a variety of techniques under a wide range of conditions. Similar experiments on F_o, V_1, and V_o may provide further insights in the near future. This chapter will review the structures of F_1, F_o, and the BFM and what has been learned about their mechanisms using single-molecule techniques. Little will be said about V-ATPase, which is very similar to ATP-synthase and almost certainly shares the same rotary mechanisms.

ATP-synthase, also known as F_1F_o-ATPase, is a ubiquitous enzyme located in mitochondria and chloroplasts of eukaryotic cells and in the cytoplasmic membranes of bacteria. It synthesizes ATP from adenosine diphosphate (ADP) and inorganic phosphate (P_i), using the IMF as the source of free energy. ATP is the "energy currency" of living organisms. Its hydrolysis to ADP + P_i releases the energy needed for many cellular processes, and it is present in relatively large amounts inside cells; ATP-synthase synthesizes roughly 2 million kg of ATP in the 75-year lifespan of a typical 70-kg human (Yoshida et al. 2001). Despite the fact that different organisms generate IMFs by many different respiratory or photosynthetic mechanisms, ATP-synthase is one of the most evolutionarily conserved enzymes (Kanazawa et al. 1981, Walker et al. 1985, Hudson et al. 1987). Under normal conditions F_o generates more torque than F_1, and thus F_1 is driven backwards to synthesize rather than hydrolyze ATP. This relationship is reversed in V-ATPase, in which rotation of V_1 drives V_o backwards to pump ions against the IMF. V-ATPase is located in many intracellular compartments (endosomes, lysosomes, secretory vesicles) and has also been identified in the plasma membrane of certain cells (Nishi and Forgac 2002, Beyenbach and Wieczorek 2006). Given that it regulates pH, a carefully controlled parameter affecting many cellular processes, V-ATPase has an important role in, for example, receptor-mediated endocytosis, protein processing and degradation, acid secretion, and bone degradation (Nishi and Forgac 2002, Beyenbach and Wieczorek 2006).

At ~50 nm in diameter and with a molecular mass of ~11 MD, the BFM is one of the largest molecular machines in bacteria. It consists of about 13 different component proteins, and a further approximately 25 proteins are required for its expression and assembly, with a total of 40–50 genes involved in expression, assembly, and control (Macnab 2003). It is a rotary machine embedded in the cell envelope and connected to an extracellular helical filament. As with F_o and V_o, the motor is powered by the flow of ions down an electrochemical gradient across the cytoplasmic membrane into the cell. The rotating filament enables the cell to swim away from unfavourable and towards favourable external conditions. Bacteria achieve active control of their motion by regulating motor rotation, the final stage of processes such as chemotaxis, phototaxis, magnetotaxis, and thermotaxis by which many species of bacteria sense and navigate their environment (Blair 1995, Falke et al. 1997, Wadhams and Armitage 2004, Baker et al. 2006, Paster and Ryu 2008). The best-studied flagellar motors are those of peritrichiously flagellated (several flagella at random locations around the cell) enteric bacteria *Escherichia coli* and *Salmonella enterica Sv typhimurium*, and results described in this review refer to one or other of these motors unless stated otherwise.

7.2. Structure

7.2.1. ATP-Synthase

ATP-synthase has a very similar overall structure whatever the source—prokaryotes, chloroplasts, or mitochondria. The overall structure of F_1F_o-ATPase has been obtained from low-resolution cryo–electron microscopy (cryo-EM) studies of yeast mitochondrial F_1F_o (Stock et al. 1999) and *E. coli* F_1F_o (Wilkens et al. 2000). Numerous atomic structures of the cytoplasmic F_1 part from various species have been obtained by X-ray crystallography, as well as a small number of structures of the membrane-bound rotor of F_o and of various other components of the enzyme. These atomic structures have been docked into a low-resolution structure of bovine heart mitochondrial ATP-synthase (Rubinstein et al. 2003), and in combination with a range of biochemical studies (e.g., Schwem and Fillingame 2006) have led to the model shown in Figure 7.1, where the main figure shows the nomenclature of the bacterial enzyme and the inset shows the equivalent mitochondrial subunits. Unless otherwise stated, we use the bacterial nomenclature in this chapter. Synthesis and hydrolysis of ATP occur in F_1, in which the minimal rotary motor consists of the stator $\alpha_3\beta_3$ and the rotor γ.

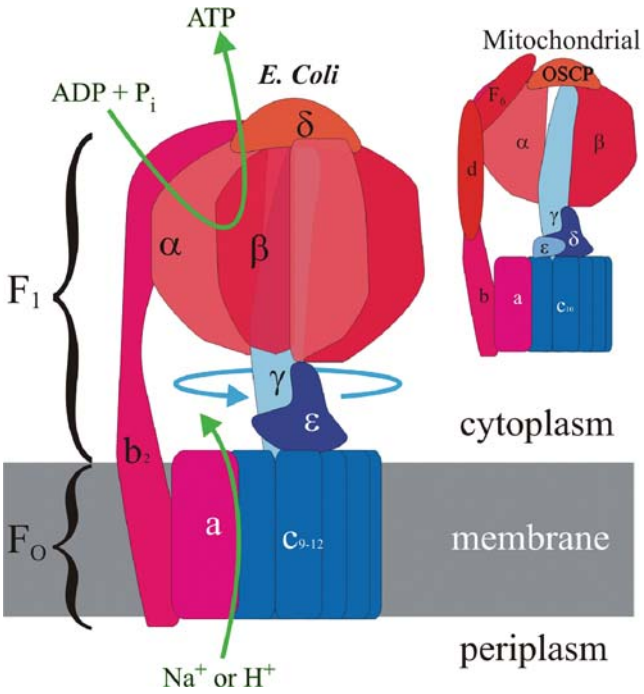

Figure 7.1. Schematic showing the structure and subunit nomenclature of *Escherichia coli* and mitochondrial **(inset)** F_1F_o-ATPase. The ε- and δ-subunits in the mitochondrial enzyme are equivalent to the ε-subunit of the *E. coli* enzyme. Rotor subunits are shown in shades of blue, stator subunits in shades of red. One α– and one β-subunit are removed in the inset to show the γ-subunit more clearly. Ion flux across the membrane in F_o drives rotation of the common rotor (blue arrow), which in turn drives synthesis of adenosine triphosphate (ATP) in F_1. ADP, adenosine diphosphate; OSCP, oligomycin-sensitivity conferring protein; P_i, inorganic phosphate

The rotor of F_o is a ring of 10–15 *c*-subunits, depending on the species (Figure 7.2), and the stator is composed of the *a*- and *b*-subunits. The peripheral stalk containing δ- and b-subunits connects the two stators, and ε helps to link the two rotors together.

F_1

Whereas the majority of single-molecule experiments on F_1 have used prokaryotic F_1, in particular from the thermophilic *Bacillus* PS3 (TF_1), most atomic structures are of the enzyme from bovine heart mitochondria. The first of these was obtained in 1994 by Walker, Leslie, and coworkers with a resolution of 2.8 Å and a crystal grown in the presence of 250 μM adenyl-5-yl imidodiphosphate (AMP-PNP; an analog of ATP), 250 μM ADP, and azide (protein data bank [PDB] code 1BMF) (Abrahams et al. 1994). The structure consists of three α-subunits, three β-subunits, and a γ-subunit. Nucleotide-binding sites were identified at the interfaces between α- and β-subunits. The three noncatalytic sites, formed mainly by the α-subunits, have AMP-PNP and Mg^{2+} bound. Of the three catalytic sites, formed mainly by β-subunits, one has ADP and Mg^{2+} bound (referred to as β_{DP}), one AMP-PNP and Mg^{2+} (β_{TP}), and one subunit is empty (β_E). The 1994 structure most likely represents the Mg-ADP inhibited form, that is, the state immediately after ATP binds the β_{TP} site, stalled by the failure of Mg-ADP release from the β_{DP} site (Hirono-Hara et al. 2001, Yasuda et al. 2003).

Several additional crystal structures were obtained subsequently, of which only a few differ significantly from the 1994 structure in terms of γ-subunit orientation or the number and location of nucleotides. One of them, bovine mitochondrial F_1 inhibited by dicyclohexylcarbodiimide (DCCD), obtained in 2000 (PDB code 1E79), has mitochondrial ε- and δ-subunits as well as the γ-subunit, forming a foot that interacts with F_o (Gibbons et al. 2000). In another bovine F_1 structure, obtained in 2001, the γ-subunit orientation is shifted by 15° compared to the 1994 structure (PDB code 1H8E) (Menz et al. 2001). This crystal was formed from aluminum fluoride–inhibited F_1 and has ADP, Mg^{2+}, and glycerol bound to all α-subunits; ADP, Mg, and SO_4^{2-} to the β_E-subunit; ADP, Mg^{2+}, and AlF_4^- to β_{DP}; and ADP, Mg^{2+}, AlF_4^-, and glycerol to the β_{TP}-subunit. It is speculated that the structure represents the post-hydrolysis, pre-product-release step, in that the β_E-subunit now binds ADP and sulfate (mimicking P_i) and adopts a "half-closed" conformation. Recently a crystal structure of bovine mitochondrial F_1 was obtained in conditions identical to those in the 1994 structure but in the absence of azide (PDB code 2CK3) (Bowler et al. 2007). The two structures differ only in the β_{DP} site. Whereas in the 1994 structure this site is occupied by ADP and azide, the 2007 structure has AMP-PNP bound. The authors take this as further evidence that the 1994 structure represents the Mg-ADP inhibited form and that the 2007 structure represents the most accurate available intermediate state in the catalytic cycle of hydrolysing F_1. In 1997, the nucleotide-free structure of the $\alpha_3\beta_3$ hexamer of TF_1 was obtained with a resolution of 3.20 Å, showing that the α- and β-subunits are essentially the same as in the bovine crystals (Shirakihara et al. 1997).

F_o

There are no high-resolution structures of the F_o stator *a*-subunit. An early X-ray structure of yeast mitochondrial ATP-synthase including F_1 and the F_o rotor showed a tenfold C-ring attached to the base of F_1 (Figure 7.2, top) (Stock et al. 1999), but without atomic resolution. In 2005 a high-resolution crystal structure of the F_o rotor, the C-ring from Na^+-ATPase from *Ilyobacter tartaricus*, was determined (Figure 7.2, bottom; PDB code

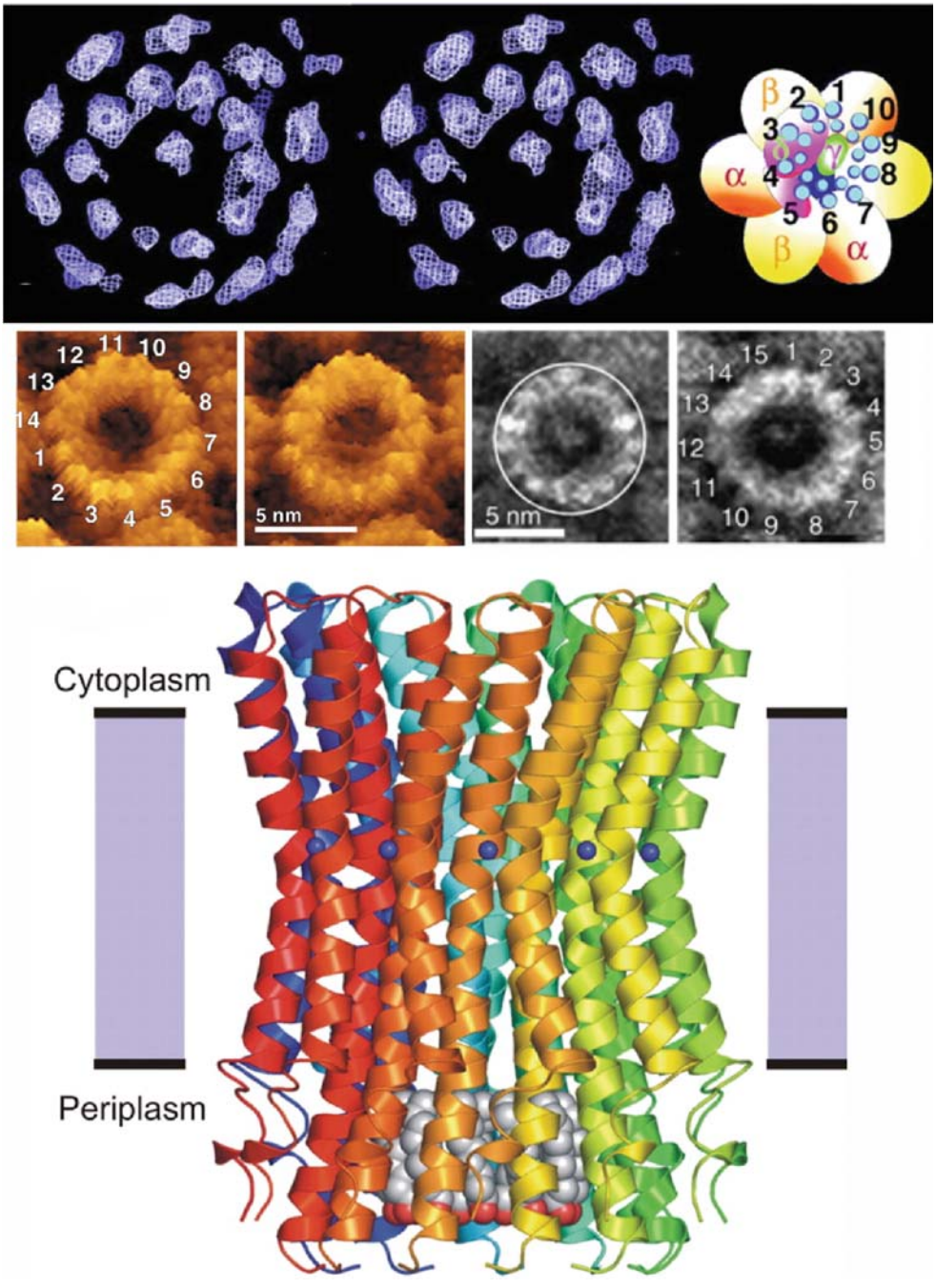

Figure 7.2. F_o rotors from various species. **Top:** Stereo views (*left*) from an electron density map of the yeast F_1c_{10} complex, and the location of the F_1 subunits in relation to the *c*-subunits (*right*). The membrane-spanning α-helices of the *c*-subunit are shown as blue circles. **Middle:** Atomic force microscope images of rotors from chloroplasts of different species, showing 11- and 15-fold symmetries. **Bottom:** X-ray crystal structure of the rotor from *I. tartaricus* showing 11 *c*-subunits. Blue spheres represent the bound Na^+ ions; detergent molecules inside the ring are shown in red and gray. [From Stock et al. (1999). top; Seelert et al. (2000), middle left; Pogoryelov et al. (2005), middle right; Meier et al. (2005), bottom; with permission.]

1YCE) (Meier et al. 2005). Each of the 11 symmetrical *c*-subunits showed a cylindrical, hourglass shape and had a Na^+ ion bound in the middle at a position predicted to be near the middle of the hydrophobic core of the membrane. A similar structure has been obtained for the rotor of a Na^+-driven V-ATPase (Murata et al. 2005), showing a tenfold symmetry, in contrast to earlier assumptions of a sixfold V_o rotor (the assumption was based on different experimental evidence—for example, chemical analysis and electron microscopy studies at lower resolution (Powell et al. 2000, Holzenburg et al. 1993, Arai et al. 1988)). The Na^+-binding sites in these structures both include a single acidic residue that could bind H^+ in a PMF-driven enzyme, indicating that H^+ rotor structures may be very similar to those of the Na^+ rotors.

One of the more interesting features of the F_o rotor is the variability of its symmetry among different species. The C-rings from yeast mitochondria, *Ilyobacter tartaricus*, *Propionigenium modestum*, *Synechocystis*, cyanobacterium, *Spirulina platensis*, and spinach chloroplasts reconstituted into two-dimensional crystals and observed with atomic force microscopy (AFM) or, in the case of *P. modestum*, observed with cryo–transmission electron microscopy (cryo-TEM), have symmetries of 10, 11, 11, 13, 14, and 15, respectively (Stock et al. 1999, Stahlberg et al. 2001, Meier et al. 2003, Pogoryelov et al. 2007, Seelert et al. 2000, Pogoryelov et al. 2005) (Figure 7.2, middle). It was suggested that the variable number of *c*-subunits within a certain species could be a regulatory mechanism (Schemidt et al. 1998), but experimental data for spinach chloroplast and *Acetobacterium woodii* ATP synthase show that the stoichiometry seems to be fixed for a given species (Fritz et al. 2008, Meyer Zu Tittingdorf et al. 2004). Given that a 360° rotation of the F_1 γ-subunit generates three ATP molecules and presumably requires each *c*-subunit to translocate one ion, it follows that the number of ions required to make one ATP molecule is not necessarily an integer. Symmetry mismatch may also be necessary for an elastic power transmission between F_1 and F_o as suggested by some (Junge et al. 2001), and it is a feature observed in the BFM as well (Thomas et al. 2006).

7.2.2. Bacterial Flagellar Motor

The bacterial flagellum spans the cell envelope, extending into the cytoplasm and the cell exterior. It consists of a hook and a flagellar filament, peptidoglycan P- and outer-membrane L-ring, rod, MS-ring, C-ring, stator units, and an export apparatus (Berg 2003, Macnab 2003). Atomic structures are available for the filament and hook, as well as for isolated protein fragments from the rotor. The overall arrangement of the motor has been derived from cryo-EM reconstructions and biochemical data and is shown in Figure 7.3. Whole rings have proved too large for X-ray crystallography. A recent report of crystallization of the membrane-spanning Mot B protein offers the hope of revealing the atomic structures of parts of the stator in the near future (O'Neill and Roujeinikova 2008).

The periplasmic P-ring and outer lipopolysaccharide membrane L-ring are composed of FlgI and FlgH proteins and transmit rotation from the motor through the cell envelope. It is not known whether they form part of the rotor or are fixed to the cell wall. The MS-ring is the first part of the motor to assemble and can be thought of as the platform on which the rest of the motor is built (Aizawa 1996, Macnab 2003). The name comes from the original idea that the ring is composed of two rings (membrane and supramembranous), but in 1992 it was shown and later confirmed that the ring consists of a single protein, FliF (Ueno et al. 1992, 1994, Suzuki et al. 2004). FliG, FliM, and FliN comprise the C-ring, which is thought to be the site of torque generation. These three proteins are often referred to as the "switch complex" because mutations lead to defects in switching (Yamaguchi et al. 1986a,b). The

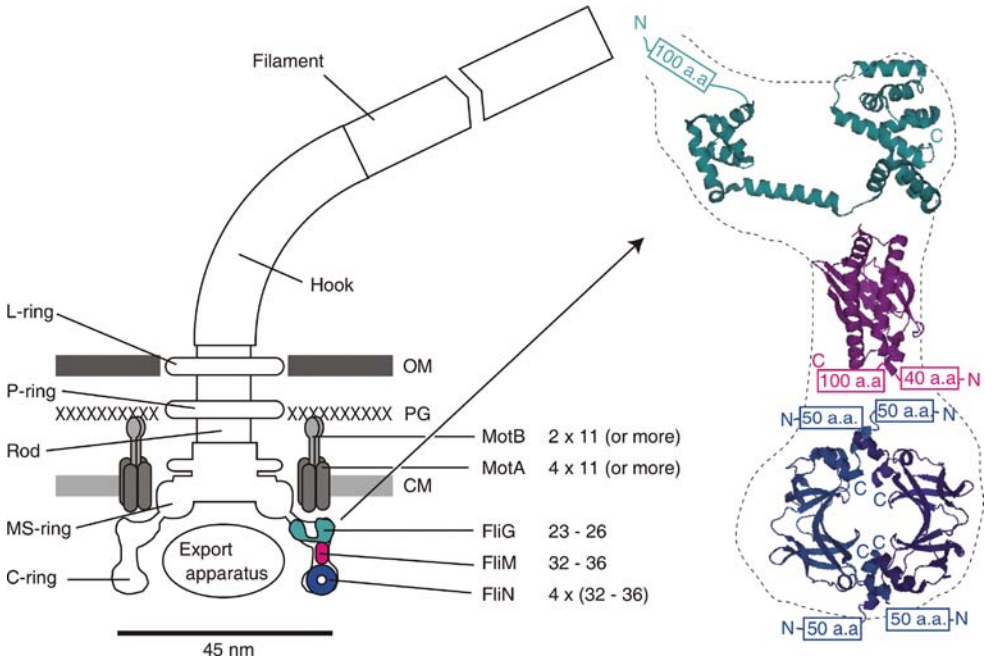

Figure 7.3. Left: Schematic side view of H^+-driven flagellar motor, with the proposed location and copy number of proteins involved in torque generation. MotA and MotB are thought to form stator complexes with stoichiometry A_4B_2, and FliN, a tetramer that has 1:1 stoichiometry with FliM. The motor spans the three layers of the of cell envelope: outer membrane (OM), peptidoglycan cell wall (PG), and cytoplasmic membrane (CM). **Right:** Detail of proposed location and orientation of rotor proteins. X-ray crystal structures of truncated rotor proteins, FliG (*cyan*; Protein Data Base [PDB] code 1LKV), FliM (*magenta*; PDB code 2HP7), and FliN (Blue; PDB code 1YAB), are shown docked into the rotor structure. The N- and C-termini and missing amino acids are indicated. a.a., amino acids. [Molecular graphics generated using PyMol (http://www.pymol.org).]

switch complex also serves as the housing for the export apparatus of the bacterial flagella. In 1999 a partial structure of *Thermotoga maritima* FliG was obtained (PDB code 1QC7) corresponding to the C-terminal domain of the protein, which functions specifically in torque generation (Lloyd et al. 1999, 1996, Irikura et al. 1993). This domain contains a set of charged residues that are essential for motor rotation and interaction with the stator (Lloyd and Blair 1997, Zhou et al. 1998a), and the structure showed these residues clustered along a ridge that is proposed to contact the stator and to change orientation to allow the motor to switch direction. The N-terminal and middle domains of FliG appear to be important for flagellar assembly and switching. In 2002 the atomic structure of a larger fragment of FliG from *T. maritima* was obtained containing the C-terminal and middle domains and an α-helix with an extended segment linking them together (Figure 7.3; PDB code 1LKV) (Brown et al. 2002). Mutational analysis from the same report indicated that FliM binds to both of these domains. An X-ray crystal structure of the middle part of *T. maritima* FliM, the protein that binds the switch-inducing signal protein CheY, was obtained in 2006 (PDB code 2HP7) (Park et al. 2006). Cross-linking studies based on this structure showed that FliM self-associates in a side-to-side arrangement, which would allow cooperative transitions during a motor switch (Park et al. 2006). Crystal structures of a fragment of FliN from *T. maritima* lacking 50 amino acids at the N-terminus were reported in 2003 (PDB code 1O6A) and 2005 (PDB code

1YAB) (Brown et al. 2005). FliN forms saddle-shaped dimers in both structures, and association studies from the same reports predict FliN tetramers and stable $FliN_4$–$FliM_1$ complexes. In the latter structure, pairs of dimers form a doughnut-shaped tetramer that has been fitted to the cryo-EM reconstruction of the bottom of the C-ring (Thomas et al. 2006). The FliG, FliM, and FliN structures from *T. maritima* provide a good model for the same proteins in *E. coli* motor due to high sequence homology overall and in particular in the segments most important for function.

Axially resolved cryo-EM of the rotor has revealed two different symmetries in the MS- and C-rings. The MS-ring and the inner part of the C-ring have 23- to 26-fold symmetry, whereas the bottom and outer parts of the C-ring are 32- to 36-fold (Thomas et al. 2006). The copy numbers of FliM and FliN have been estimated as 34 ± 6 and 111 ± 13, respectively (Thomas et al. 1999, Zhao et al. 1996), consistent with a $\sim$34 copies of an M_1N_4 unit. FliF–FliG fusion proteins produce functional motors (Kihara et al. 2000), suggesting that FliG shares the symmetry of the MS- rather than that of the C-ring. In one model, FliG is restricted to the inner part of the C-ring, with $\sim$26-fold symmetry (Thomas et al. 2006). In an alternative model (Brown et al. 2007), FliG spans the inner and outer parts of the C-ring, and the outer part has *n* defects, where *n* is the difference between the two symmetries and each defect is a missing FliG. A similar symmetry mismatch was proposed earlier in a model in which *n* was identified with eight stator units and each unit generated torque by propagating the defect along the ring (Thomas et al. 1999). The model predicts that the MS- and C-rings rotate at different speeds, an outlandish proposal that might be testable in future using fluorescent-labelled rotor proteins.

MotA and MotB are membrane proteins that form the stator of the H^+-driven motor, and PomA and PomB are the Na^+-driven equivalents, with additional proteins MotX and MotY required in wild-type Na^+ motors. Mot (or Pom) proteins can be inserted into the assembled structure by inducing the *mot* genes. Based on Na^+-driven–motor studies, PomA and PomB proteins form a complex of four PomA and two PomB (the same is likely for MotA and MotB) proteins (Sato and Homma 2000, Yorimitsu et al. 2004). Two thirds of MotA is in the cytoplasm (Blair and Berg 1991, Zhou et al. 1995), and MotB has one membrane-spanning α-helix and the rest of the molecule is in the periplasm (Chun and Parkinson 1988). MotB has a peptidoglycan-binding domain near the C-terminus, which anchors the stator unit to the cell wall (de Mot and Vanderleyden 1994). Mutational studies identified Asp32 in MotB (of *E. coli*) as an essential proton-accepting residue that is presumed to form part of the conduction pathway in the motor (Zhou et al. 1998b).

A recent complete EM structure *in situ* of the flagellar motor of the spirochete *Treponema primitia* at 7-nm resolution (Murphy et al. 2006) shows a motor of different shape and size from that previously reported in *S. typhimurium* (Thomas et al. 2006). Sixteen stator units are visible, each connected to the P-collar, and in three places to the rotor. Only one of these latter connections corresponds to the part of the C-ring where FliG is thought to be located in the rotor of *S. typhimurium* (Thomas et al. 2006).

7.3. Single-Molecule Methods for Measuring Rotation

The earliest measurement of the motion of a single molecular motor was the tethered bacterial cell experiment of Silverman and Simon (1974), in which a single BFM was tethered to a microscope coverslip by the filament and the whole cell was used as a visible marker of rotation. Since then, a range of markers has been used to measure rotation of the BFM, F_1,

and F_1F_o: polystyrene beads, fluorescent actin filaments, magnetic beads, gold nanoparticles, and single fluorescent molecules. In single-molecule experiments on rotary motors, motor torque M is balanced by viscous drag on the marker, $M = f\omega$, where f is the frictional drag coefficient of the marker and ω is its angular velocity (the Reynolds number for a spinning motor is much less than 1, and therefore inertial effects can be neglected). External torque has also been applied to tethered cells using electrorotation, to magnetic beads using magnetic fields, and to polystyrene beads and tethered cells using optical tweezers. These methods and their applications will be briefly summarized here.

7.3.1. ATP-Synthase

Although indirect evidence of rotation in F_1 had been obtained before (Rao and Senior 1987, Boyer 1993, Duncan et al. 1995, Sabbert et al. 1996, Abrahams et al. 1994), direct observation of rotation came in 1997 (Noji et al. 1997). A genetically engineered TF_1 with His tags on β-subunits and a Cys mutation on the γ-subunit was attached to a coverslip surface via nickel nitrilotriacetic acid (NTA), and a fluorescently labelled actin filament was attached to the γ-subunit through a biotin-streptavidin link (Figure 7.4A). Direct rotation was observed under an epifluorescence microscope. The same method was used for the observation of three ATP-dependent steps in motor rotation at low ATP concentration [ATP] (Yasuda et al. 1998). Greater temporal resolution was achieved with a much smaller marker of rotation, a 40- to 300-nm gold bead or bead pair attached to TF_1 (Figure 7.4B) observed with a high-speed video camera at 8,000 frames per second and laser dark-field (DF) microscopy (Yasuda et al. 2001). From these experiments it became clear that with an ∼100-nm gold bead pair or smaller the motor rotation is no longer impeded by the load and reaches a maximum speed in saturating [ATP] at room temperature of ∼130 Hz. By comparison, the motor speed with actin filaments attached varied from ∼0.1 to 7 Hz. The gold bead experiment allowed observation of ∼2-ms substeps that are [ATP] independent and therefore could not easily be slowed down by using low [ATP]. In a later experiment the angular resolution was increased by using 200-nm bead pairs instead of single beads (Shimabukuro et al. 2003). Various single-molecule fluorescence methods have also been used for low-resolution studies of TF_1 rotation—for example, polarized fluorescence microscopy of single fluorophores attached to the γ-subunit (Figure 7.4C) (Adachi et al. 2000) and fluorescence resonance energy transfer (FRET) between a donor attached to one of the β-subunits and an acceptor on a γ-subunit (Figure 7.4D) (Yasuda et al. 2003). Binding of a fluorescent ATP analog to F_1 has also been observed simultaneously with rotation of a bead pair attached to the γ-subunit (Nishizaka et al. 2004).

Rotation of F_1 from *E. coli* (EF_1) has been observed using fluorescent actin filaments (Omote et al. 1999, Iko et al. 2001), gold beads (Nakanishi-Matsui et al. 2006, 2007), and back-focal-plane interferometry of polystyrene bead pairs (Pilizota et al. 2007). The maximum observed speed of EF_1 with 60- and 40-nm gold beads attached to the γ-subunit is 400–500 Hz (Nakanishi-Matsui et al. 2006). The relatively low speed of TF_1 at room temperature reflects the high temperature of its native conditions and makes resolution of the details of stepping rotation considerably easier than in EF_1. EF_1 rotation has also been observed in laser DF microscopy via intensity changes in polarized light scattering by gold nanorods (Spetzler et al. 2006, York et al. 2007).

Synthesis of ATP by externally rotated F_1 was demonstrated in 2004 (Itoh et al. 2004) and again with improved resolution in 2005 (Rondelez et al. 2005). F_1 was attached to the coverslip surface by engineered His tags on β-subunits as before, and the γ-subunit was

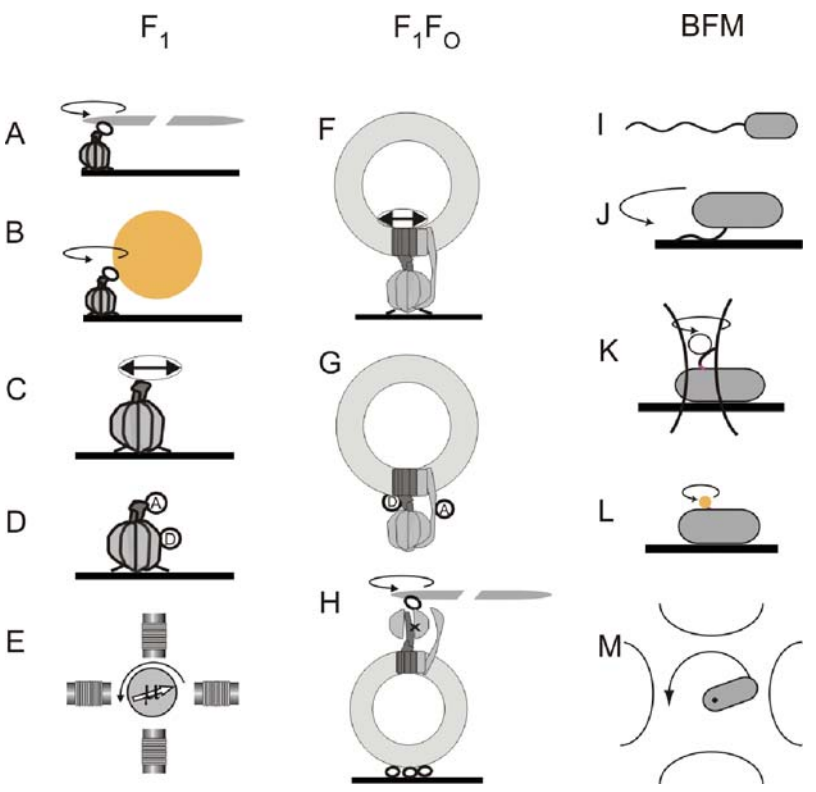

Figure 7.4. Single-molecule assays for rotary motors. The F_1 rotation has been measured by attaching α- or β-subunits to the surface via His-tags and attaching to the γ-subunit, via biotin-avidin, **(A)** fluorescent actin filaments, **(B)** beads, **(C)** single fluorophores, or **(E)** magnetic beads. Fluorescence resonance energy transfer (FRET) has also been used to determine the relative positions of γ- and β-subunits during rotation **(D)**. F_1F_o rotation driven by energized F_o in phospholipid vesicles has been observed via single fluorophores **(F)**, FRET **(G)**, and actin filaments **(H)**. Rotation of the BFM has been measured using **(I)** swimming cells, **(J)** tethered cells, **(K)** polystyrene beads attached to flagella, and **(L)** gold beads attached to hooks. External torque has been applied to F_1 using magnetic fields **(E)** and to the bacterial flagellar motor (BFM) using tethered cells and either electrorotation **(M)** or optical tweezers. More details of these methods can be found in the text.

labelled with a superparamagnetic bead attached via a biotin-streptavidin link (Figure 7.4E). The magnetic bead was rotated using magnetic tweezers, resulting in production of ATP. Typical resolutions reported using magnetic beads are several seconds and 5° (Hirono-Hara et al. 2005). Pairs of polystyrene beads each 500 nm in diameter have also been used as handles to apply external torque to F_1 with an optical trap in an "angle clamp" feedback mode (Pilizota et al. 2007) with a bandwidth up to 1.6 kHz and angular precision of 2°. The drawback of the method is the considerable variation in the trap stiffness with angle and bead pair. Whereas in principle optical tweezers are easier to calibrate due to the good reproducibility of polystyrene beads compared to magnetic beads, the method in fact gave no great improvement in calibration of absolute torque compared to magnetic tweezers.

The rotation of isolated F_o has not been measured directly. There are several reports of F_1F_o rotation measured in a similar manner to the TF_1 and EF_1 experiments (Sambongi et al. 1999, Nishio et al. 2002). Although F_o was present in these experiments, it was not energized, making them effectively F_1 rotation measurements, confirming the co-rotation of F_1 and

F_o rotors. Low-resolution measurements of F_1F_o rotation driven by F_o have been reported. The first observation of F_1F_o rotation during ATP synthesis or hydrolysis came in 2002 (Kaim et al. 2002). Na^+-translocating ATP-synthase of *P. modestum* specially labelled with a single fluorophore on one *c*-subunit was used. The enzyme was immobilized via His tags on β-subunits and reconstituted into proteoliposomes (Figure 7.5F). Rotation was observed with polarization-resolved confocal microscopy during synthesis. In a later experiment F_1F_o from *E. coli* was engineered for FRET, with a donor on the γ- or ε-subunit and an acceptor on the *b*-subunit, and incorporated into liposomes (Figure 7.5G). This allowed the detection of rotation during both synthesis and hydrolysis (Borsch et al. 2002, Diez et al. 2004, Zimmermann et al. 2005). A variant of the F_1 actin experiment has also been reported in which TF_1 was reconstituted with bacteriorhodopsin and *E. coli* F_1F_o in phospholipid vesicles. TF_1 was locked using azide and freed from the F_o stator by removal of the δ-subunit and labelled with an actin filament on the β-subunit (Figure 7.4H) (Zhang et al. 2005). When the vesicles were illuminated, the actin filaments rotated, indicating rotation of F_o driven by the PMF generated by proton pumping in bacteriorhodopsin.

7.3.2. Bacterial Flagellar Motor

True rotation of bacterial flagella, as opposed to propagation of helical waves, was demonstrated in the 1970s (Berg and Anderson 1973, Silverman and Simon 1974). Cells were tethered to a microscope coverslip by filaments (Figure 7.4 J), and rotation of the cell body was observed in a light microscope (Silverman and Simon 1974). A nonswimming strain with straight filaments was used to exclude the possibility that cells were swimming about an inert point of attachment rather than by a rotating motor. To observe the faster rotation of the motor (tethered cells rotate at up to 20 Hz) when driving smaller loads, several techniques have been used.

The rotating filaments of stuck or swimming cells (Figure 7.4I) have been visualized with conventional DF, laser DF, differential interference contrast (DIC), and fluorescence microscopy. Conventional DF and DIC studies have been limited to video rates (Block et al. 1991, Hotani 1976, Macnab 1976). Laser DF has achieved higher time resolution by recording the oscillating light intensity passing through a slit perpendicular to the image of a single filament, which appears as a series of bright spots in this method—one spot for each turn of the filament helix (Kudo et al. 1990, Muramoto et al. 1995). The maximum recorded speed of any molecular motor, 1,700 Hz in the Na^+-driven motor in *Vibrio alginolyticus* at 37ºC, was measured using this technique (Magariyama et al. 1994). Fluorescent labelling of flagellar filaments combined with stroboscopic laser illumination and high-speed video microscopy has revealed polymorphic transitions of filaments (Turner et al. 2000) both in swimming cells (Darnton et al. 2007) and in response to external forces applied with optical tweezers (Darnton and Berg 2007).

The preferred method of measuring fast rotation since 2000 has been to attach polystyrene beads, 200 nm to 2 μm in diameter, to truncated flagellar filaments of immobilized cells. Beads have most commonly been tracked by back-focal-plane interferometry (Figure 7.4 K) (Ryu et al. 2000, Chen and Berg 2000a, b, Sowa et al. 2003, 2005, Reid et al. 2006, Lo et al. 2006, 2007, Inoue et al. 2008). In addition, 200-nm fluorescent beads have been tracked by fluorescence microscopy, and bead tracking has allowed resolution of 26 steps per revolution in very slow flagellar rotation (Sowa et al. 2005). The angular resolution of bead or tethered assays is estimated to be better than 1°, but time resolution is limited to milliseconds or worse by the relaxation time of the flexible hook (Block et al. 1989, Sowa et al. 2005). In

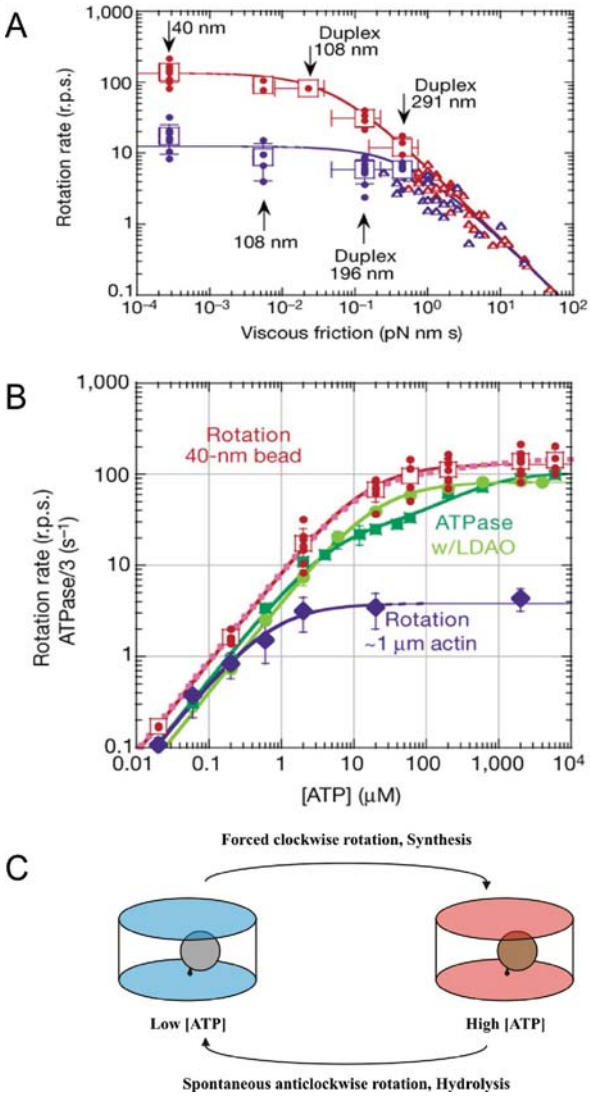

Figure 7.5. **A**. Average speeds of different rotating markers attached to F_1 at saturating concentration of adenosine triphosphate [ATP] (2 mM; *red*) and low [ATP] (2 μM; *blue*) versus rotational frictional drag coefficient. Lines show the expected speeds for a motor producing a constant torque of 40 pN nm rad^{-1}. **B**. Average speeds of 40-nm gold beads (*red*) and actin filaments (*blue*) attached to F_1 versus [ATP]. ATP hydrolysis rates by free F_1, divided by 3 for comparison with rotation rates assuming three ATP molecules hydrolysed per revolution, are shown in green with and without LDAO that prevents occupation of the ADP-inhibited state. Curves show fits with Michaelis-Menten kinetics. **C**. ATP synthesis by single F_1 molecules enclosed in microchambers and driven to rotate by magnetic beads. ATP synthesis was detected as an increase in rotation speed when the magnetic field was removed, due to the increase in [ATP] within the chamber. [Panels A and C from Yasuda et al. (2001), with permission.]

2008, higher time resolution was achieved by using 60-nm gold beads attached to the flagellar motor via the hook in a bacterial strain lacking filaments (Figure 7.4L). Rotation of the bead was observed with laser DF in a manner similar to the F_1 experiments (Yuan and Berg 2008). The viscous drag coefficient of the gold bead is at least two orders of magnitude smaller than any previously measured, making it essentially indistinguishable from zero load. Although the relaxation time of the hook with a 60-nm gold bead attached is estimated to be less than 6 μs, the angular resolution in these experiments was too low to reveal details of rotation within a single revolution.

Early attempts to use magnetic particles to apply external torque to tethered cells were abandoned because they were unable to apply sufficiently large torque (Berg HC, personal communication). Instead, a technique called electrorotation has been used (Washizu et al. 1993, Berg and Turner 1993). Microelectrodes arranged in a cross with a gap of ~70 μm generate a rotating electric field that polarizes a cell located in the gap (Figure 7.4 M). The polarization of the cell falls behind the rotating field, and a torque is generated as the dipole tries to line up with the field. Using substantial voltages, it was possible to spin the cell body in both directions at speeds up to ~1 kHz. Early electrorotation experiments indicated a ratchet-like mechanism in which considerably more torque is needed to force the motor backwards than to stop it rotating forwards (Berg and Turner 1993), but later work showed this to be an artefact of the method (Berry and Berg 1996, 1999, 1997, Berry et al. 1995). Optical tweezers have also been used to exert external torque on the motor with a tethered cell body or beads (Berry and Berg 1997, Pilizota et al. 2007). The motor torque of tethered cells was similar when they were rotated very slowly in either direction by optical tweezers, confirming the electrorotation results (Berry and Berg 1997). The BFM has also been controlled with optical tweezers and pairs of 0.5-μm beads, as described for F_1 in the previous section (Pilizota et al. 2007).

7.4. Energy Transduction

7.4.1. ATP-Synthase

ATP-synthase uses IMF as its free energy input and produces ATP from ADP + P_i as its output. However, single-molecule studies on the whole coupled enzyme are very few, and we will therefore consider the motors F_1 and F_o separately in this section. Considering each as a rotary motor, the inputs are IMF for F_o and ATP hydrolysis for F_1, and the output in both cases is torque. In ATP-synthase it is predicted that the torque generated by F_o should be higher than that generated by F_1, so that F_1 is driven in reverse and ATP is synthesized. In addition, the difference in torques should be small, so that most of the work done by F_o is used to synthesize ATP rather than being wasted as heat. This appears to be true across a range of species, in which the C-ring symmetry and thus the number of ions coupled to each ATP molecule vary proportionally with the ratio of free energies of ATP hydrolysis and ion transit (D. Muller, personal communication). A compliant elastic coupling between F_1 and F_o is believed to be necessary to smooth over the different step sizes of the two motors (see later discussion), transiently storing the energy output of three to five ions passing through F_o for each ATP synthesized.

F_o

F_o uses IMF as the source of free energy needed to drive the rotation of its rotor parts (Mitchell 1961, 1966, Jagendorf and Uribe 1966). The free energy available when an ion such

as H^+ or Na^+ crosses an energized membrane is defined as the product of the IMF and the ionic charge. IMF includes electrical and chemical potentials and is defined as follows:

$$\mathrm{IMF} = \Delta\psi + \frac{k_\mathrm{B}T}{q}\ln\left(\frac{C_\mathrm{i}}{C_\mathrm{o}}\right) \tag{7.1}$$

where $\Delta\psi$ is the difference in electrical potential between the inside and outside of the cell (i.e., the membrane potential), k_B is Boltzmann's constant, T is the absolute temperature, $k_\mathrm{B}T$ is the thermal energy, q is the charge of the ion, and C_i and C_o are the respective activities of the ions inside and outside the cell.

Early estimates of the proton conductance of F_o varied over four orders of magnitude due to difficulties in estimating the number of active molecules (Negrin et al. 1980, Friedl and Schairer 1981, Schneider and Altendorf 1982, Sone et al. 1981, Lill et al. 1986, Althoff et al. 1989, Wagner et al. 1989). The difficulty was resolved by preparing small chromatophore vesicles from the photosynthetic bacterium *Rhodobacter capsulatus*, which would on average contain less then one copy of F_o (Feniouk et al. 2001, 2002, 2004). Thus, it was determined that maximum conductance of F_o is 10 fS (at pH 8), equivalent to translocating 6,500 protons sec^{-1} at 100 mV (Feniouk et al. 2004). In the bacterial cytoplasmic membrane $\Delta\psi$ is typically in the range 120–150 mV (Nicholls and Ferguson 2002, Lo et al. 2007, Berg 2003, Felle et al. 1980, Kashket et al. 1980, Shioi et al. 1980), corresponding to (4–6)$k_\mathrm{B}T$ per ion, and the total IMF is typically in the range 150–200 mV. For different systems, for example, mitochondria, IMF varies within the same range (Nicholls and Ferguson 2002). Given these values, an upper limit for the torque produced by F_o can be estimated as $M = (Nq\cdot\mathrm{IMF})/2\pi$, where $N \approx 10$ is the number of ions coupled to one revolution, assumed to be the same as the F_o rotor symmetry. Thus we estimate that F_o can generate up to ~50 pN nm rad^{-1} of torque. The only reported measurement of F_o rotation, using an actin filament and reconstituted F_1F_o in anchored phospholipid vesicles (Zhang et al. 2005) (Figure 7.4H), estimated a torque of ~28 pN nm rad^{-1}. However the PMF in this experiment was not known, and it is also possible that the speed of the actin filament, from which the torque was estimated, is slower than the speed of F_o rotation due to rotation of F_o in the membrane or shearing rotational flow within the vesicle.

F_1

The first direct proof of rotation in F_1 coupled to ATP hydrolysis came in 1997, with the rotating actin filament experiment described in Section 7.3.1. Similar results were subsequently obtained using an actin filament to label the ε-subunit of TF_1 (Kato-Yamada et al. 1998), the γ-subunit of EF_1 (Iko et al. 2001), the *c*-, α-, and β-subunits of EF_1F_o (Sambongi et al. 1999, Tanabe et al. 2001), and the *β*- or *a*-subunit of EF_1F_o in a nonenergized membrane fragment (Nishio et al. 2002). These experiments all confirm the rotational mechanism illustrated in Figure 7.1.

The free energy available from the hydrolysis of one ATP molecule is given by

$$\Delta G = \Delta G_0 + k_\mathrm{B}T\ln\left(\frac{[\mathrm{ATP}]}{[\mathrm{ADP}]\cdot[\mathrm{P_i}]}\right) \tag{7.2}$$

where ΔG_0 is the standard free energy and [X] represents the molar concentration of chemical species *X*. The energy released by one ATP molecule is $\Delta G = 57$ kJ/mol ≈ 95 pN nm (Berg

et al. 2002), setting the upper limit to the torque generated by F_1 as $M_{max} = (3 \cdot \Delta G)/2\pi \approx 45$ pN nm rad^{-1}. As expected, this is a little lower than the predicted maximum torque of F_o. The 1997 experiment (Noji et al. 1997) found that actin filaments a few microns long attached to the γ-subunit of TF_1 rotated at approximately up to ~4 Hz in saturating [ATP]. The average torque generated by each filament was estimated by multiplying this speed by the rotational drag coefficient of the filament, ζ, estimated as (Yasuda et al. 1998)

$$\zeta = \frac{(4\pi/3)\eta L^3}{\ln(L/2r) - 0.447}$$

where η is the viscosity of the medium, r is the radius, and L is the length of the filament. Torques up to ~40 pN nm rad^{-1} were estimated, consistent with the predictions based on the energetics of ATP hydrolysis and IMF. In 2001 the torque of the motor was calculated from the actin filament curvature, based on the finding that the major resistance of the actin filament to the rotation of the motor comes from viscous and other interactions with the surface. The value obtained was ~50 pN nm rad^{-1} (Pänke et al. 2001, Cherepanov and Junge 2001).

These results are therefore consistent with the hypothesis that one ATP is hydrolysed per 120° revolution and the motor operates near ~100% efficiency at low speeds when driving a large viscous load with nanomolar to millimolar [ATP] (Sakaki et al. 2005). In 2001 a much improved F_1 rotation experiment using gold beads instead of actin filaments (Yasuda et al. 2001) mapped the dependence of rotation rate upon viscous load and [ATP] (Figure 7.5A, B). In saturating [ATP] with gold beads 100 nm or less in diameter, speed was independent of both bead size and [ATP], indicating a rate-limiting chemical step linked to ATP hydrolysis. With larger viscous loads speeds were reduced, indicating rate-limiting mechanical rotation of the γ-subunit and attached load under these conditions. For the smallest loads, the speed versus [ATP] relationship followed Michaelis-Menten kinetics with similar V_{max} and K_m as measured for ATP hydrolysis in bulk by unlabelled F_1, demonstrating that the attached gold particle did not affect the kinetics of ATP hydrolysis. Compared to rotation rates, the bulk hydrolysis rate is ~40% too low, presumably due to an inactive fraction in the bulk assay.

Direct evidence of mechanically driven ATP synthesis, with F_1 rotation driven externally by a magnetic bead rather than by F_o, came in 2004 (Itoh et al. 2004) and 2005 (Rondelez et al. 2005). Detecting the small quantities of ATP synthesized proved to be the most difficult part of these experiments due to contaminating ATP in buffers nominally containing only ADP. The key was to confine the experiment to a small volume so that the small number of ATP molecules synthesized constituted a measurable increase in ATP concentration. In 2004, ATP was detected by the luciferase–luciferin reaction in droplets 3 μm high by 30 μm in diameter. The 2005 experiment used a silicone device presenting a large array of cavities 1.5 μm high by 1.1 μm in diameter, and ATP was detected via the concentration-dependent increase in speed of the very same F_1 molecule that was used to synthesize it, after the external magnetic field was switched off (Figure 7.5c). Tight coupling between ATP synthesis and rotation in this experiment was dependent upon the ε-subunit: magnetic beads attached to $\alpha_3\beta_3\gamma\varepsilon$ synthesized an average of 2.3 ± 1.6 ATP molecules per rotation, a coupling efficiency of ~77%, whereas with $\alpha_3\beta_3\gamma$ the coupling efficiency fell to 17%. The torque required to synthesize ATP was not measured.

7.4.2. Bacterial Flagellar Motor

Input

The BFM, like F_o, is powered by the IMF across the bacterial cytoplasmic membrane. The first direct evidence for this was the observation of flagellar rotation in starved *Streptococcus* or *Bacillus subtilis* cells provided with an artificial membrane potential or pH gradient and no ATP (Manson et al. 1977, Matsuura et al. 1977), confirming earlier indications that the motor was ion driven (Larsen et al. 1974). The existence of Na^+-driven motors in alkalophilic *Bacillus* and in *Vibrio* species was demonstrated shortly after. Flagellar motility of these species was sensitive to Na^+ concentration changes and not sensitive to proton ionophores that collapse the PMF (Chernyak et al. 1983, Hirota and Imae 1983, Hirota et al. 1981). Numerous functional chimeric motors that mix components from motors with different driving ions support the conclusion that the mechanisms of Na^+- and H^+-driven motors are very similar (Asai et al. 2003, Yorimitsu et al. 2003). The pattern of ion selectivity of functional chimeric motors shows that no single component of the motor uniquely determines ion selectivity (Sowa and Berry 2008).

Single-molecule experiments in the BFM are made easier than in F_o by the very same factors that make them harder than in F_1. Live bacteria present a motor that is assembled in an energized membrane, anchored to the cell wall, and relatively easy to label via the hook or filament that extends from the cell. Thus, in contrast to F_o, ion-driven rotation in the BFM can be observed simply by sticking live cells to a surface and measuring the rotation of a marker attached to hook or filament. However, unlike with F_1, where ATP, ADP and P_i can be added at whatever concentrations are desired, the energy input to the BFM is linked to the metabolic state of the cell and therefore relatively difficult to measure and control. There have been two approaches to this problem: Externally impose an IMF using voltage clamping, diffusion potentials, and specified concentration gradients in combination with ionophores; or disrupt the natural energization of the cell and attempt to measure the resulting IMF.

The most definitive experiment to impose an IMF on the flagellar motor was performed by Fung and Berg (1995). Filamentous cells were drawn halfway into micropipettes, the cytoplasmic membrane of the part inside the pipette was made permeable by exposure to a proton ionophore, and the external part of the membrane was energised by voltage clamping the pipette. Dead cells were used to mark motors in the external part, imposing a high viscous load equivalent to a tethered cell, and speed was found to be proportional to $\Delta\psi$ up to –150 mV (Figure 7.6A). This result confirmed earlier measurements of the speed of the tethered gram-positive bacteria *Streptococcus* and *Bacillus* energized by a K^+ diffusion potential (Figure 7.6B) (Khan et al. 1985, Manson et al. 1980, Meister and Berg 1987). The independent effects of each term in the IMF, Eq. (7.1), were investigated in tethered *Streptococcus* cells in 1980 using ionophores and uncouplers (Manson et al. 1980). Both $\Delta\psi$ and pH gradient were found to be equivalent in driving the motor (Manson et al. 1977, 1980); the speed depended only on the size of the PMF, not how it was composed. The dependence of motor speed on PMF at low load has been measured only by disrupting natural energization. Gabel and Berg (2003) attached polystyrene beads 0.4 μm in diameter to the free rotating filament of tethered cells and gradually collapsed the PMF by adding low concentrations of the proton ionophore carbonyl cyanide *m*-chlorophenylhydrazone (CCCP) (Figure 7.6C). In each cell the speed of the motor rotating the bead (low load) was found to be proportional to that of the tethered motor (high load). Tethered cell speed is proportional to PMF, and thus it was concluded that

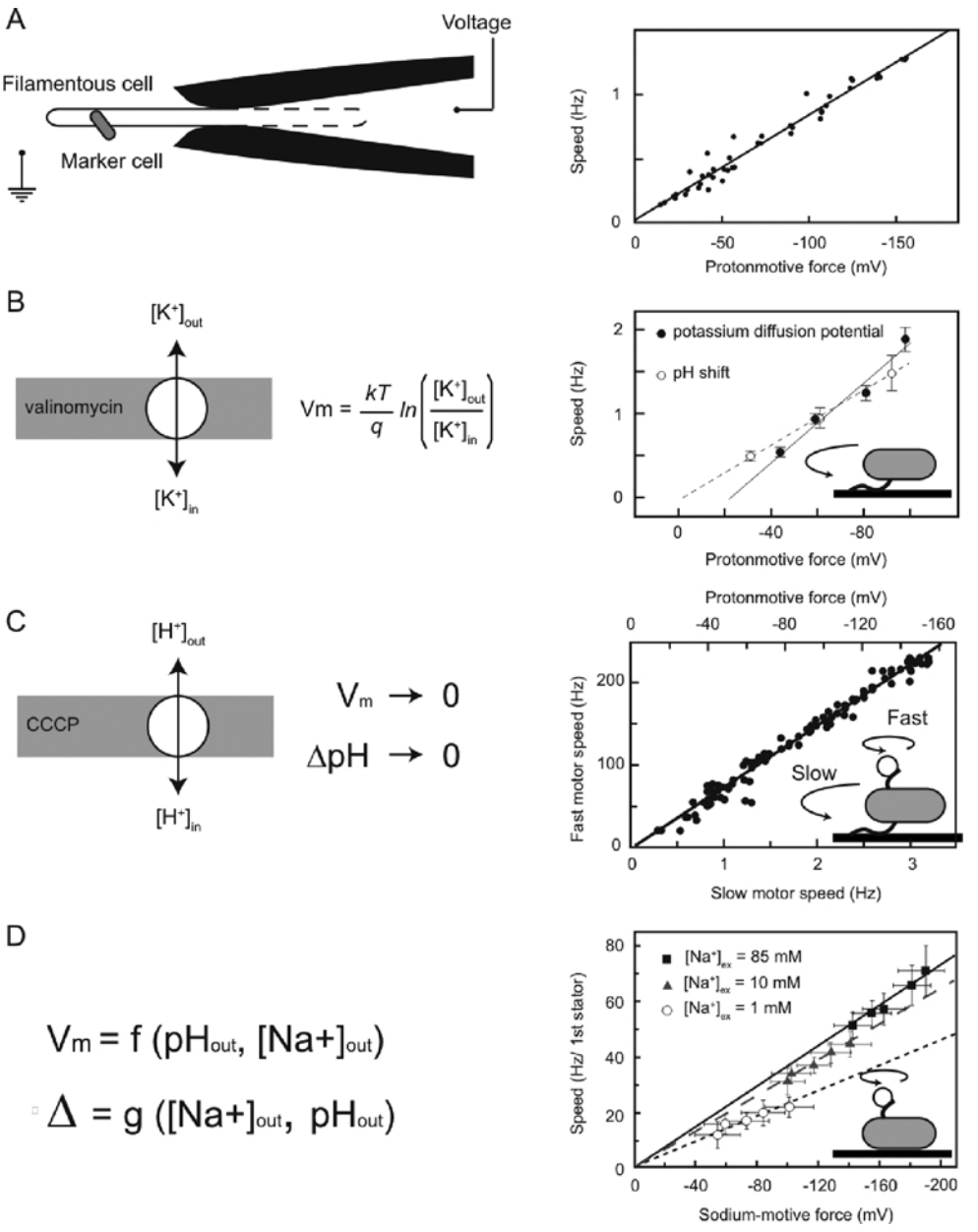

Figure 7.6. Torque versus ion-motive force in the BFM. **A. Left:** Schematic of a voltage clamp method using filamentous *Escherichia coli* cells held in custom-made micropipettes. The part of the membrane inside the pipette (*dashed line*) is made permeable using the ionophore gramicidin S. Motor speed was monitored by videomicroscopy of a dead cell attached to the motor. **Right:** Motor speed is proportional to membrane voltage (= protonmotive force [PMF]) between 0 and –150 mV. **B. Left:** Membrane voltages in *Streptococcus* can be controlled by a K^+ diffusion potential in the presence of valinomycin. **Right:** The speed of tethered *Streptococcus* cells is proportional to the PMF, and membrane voltage is equivalent to the pH gradient under these conditions. **C. Left:** The PMF can be varied slowly from –150 mV down to zero by adding small concentrations of carbonyl cyanide *m*-chlorophenylhydrazone (CCCP) or sodium azide. **Right:** Based on the result of panel A, the speed of a tethered *E. coli* motor (lower axis)

motor speed at low load is also proportional to PMF, although the relative contributions of $\Delta\psi$ and pH gradient were not known.

In 2006 and 2007, the effects of both components of SMF on motors were measured at high (1-μm beads) and low (0.36-μm beads) load (Lo et al. 2006, 2007) in chimeric sodium-driven flagellar motors in *E. coli* (Asai et al. 2003, Sowa et al. 2005, Lo et al. 2006). The $\Delta\psi$ was varied by changing external pH and the $[Na^+]$ gradient (ΔpNa) by changing external $[Na^+]$. The $\Delta\psi$ and intracellular $[Na^+]$ were measured in single cells using two different fluorescent dyes (Lo et al. 2006, 2007). At high load, motor speed was proportional to SMF, with equivalent contributions from ΔpNa and $\Delta\psi$ as for PMF in previous work. The linear dependence of speed and IMF in the high-load regime, where load rather than electrochemical processes such as the arrival of ions is rate limiting, is consistent with high efficiency and tight coupling. At low load, however, the components of SMF were not equivalent (Lo et al. 2007). At a given external $[Na^+]$, speed was proportional to SMF, but the proportionality constant changes depending on the sodium concentration. Higher $[Na^+]$, corresponding to a larger relative ΔpNa contribution to the SMF, gave a larger constant of proportionality (Figure 7.6D). This result is consistent with an earlier experiment on the sodium-driven *V. alginolyticus* motor (Sowa et al. 2003) and indicates that in the low-load regime ion binding is the rate-limiting step.

The only measurement of the ion flux through the flagellar motor was based on shifts in the rate of pH change of a weakly buffered dense suspension of swimming *Streptococcus* cells when motors were stopped by cross-linking their filaments with antifilament antibody (Meister and Berg 1987). The estimated flux was on average 1,240 ± 240 protons per revolution per motor over a speed range of ∼20–60 Hz (Meister and Berg 1987).

Output

Torque and rotation are the output of the BFM. The recent detection of steps in motor rotation (see section Interactions between Rotor and Stator) promises to offer deep insight into the motor's mechanochemical cycle in the near future. However, at the time of writing, the best way of understanding the motor has been by investigating its torque–speed relationship. Torque measurements have been made at a range of speeds, using several different techniques. The results are summarized in Figure 7.7. Measurements on tethered *Streptococcus* cells gave a linear torque–speed relationship (Manson et al. 1980, Lowe et al. 1987). However, later experiments using polystyrene beads attached to truncated filaments achieved higher temporal resolution with a broader range of applicable loads. Load on the motor was changed by varying the size of the bead and using unlabelled filaments for the lowest load point, or more reliably by using a small bead and varying the viscosity of the medium (Ryu et al. 2000, Chen and Berg 2000a, Sowa et al. 2003, Inoue et al. 2008). The motor torque is approximately

Figure 7.6. (continued) was used as a proxy for PMF (upper axis, absolute value shown). The speed of a second motor on the same cell, attached to a submicron bead, was found to be proportional to PMF. **D. Left:** Both components of the sodium-motive force (SMF) in *E. coli* can be varied using external pH and Na^+ concentration and quantified using fluorescence methods. **Right:** The speed of single-stator chimeric motors driving small loads is proportional to the SMF at a given external Na^+ concentration, but motors spin faster in high Na^+ even at the same SMF. [Data adapted from (A) Fung and Berg (1995), (B) Manson et al. (1980), (C) Gabel and Berg (2003), and (D) Lo et al. (2007).]

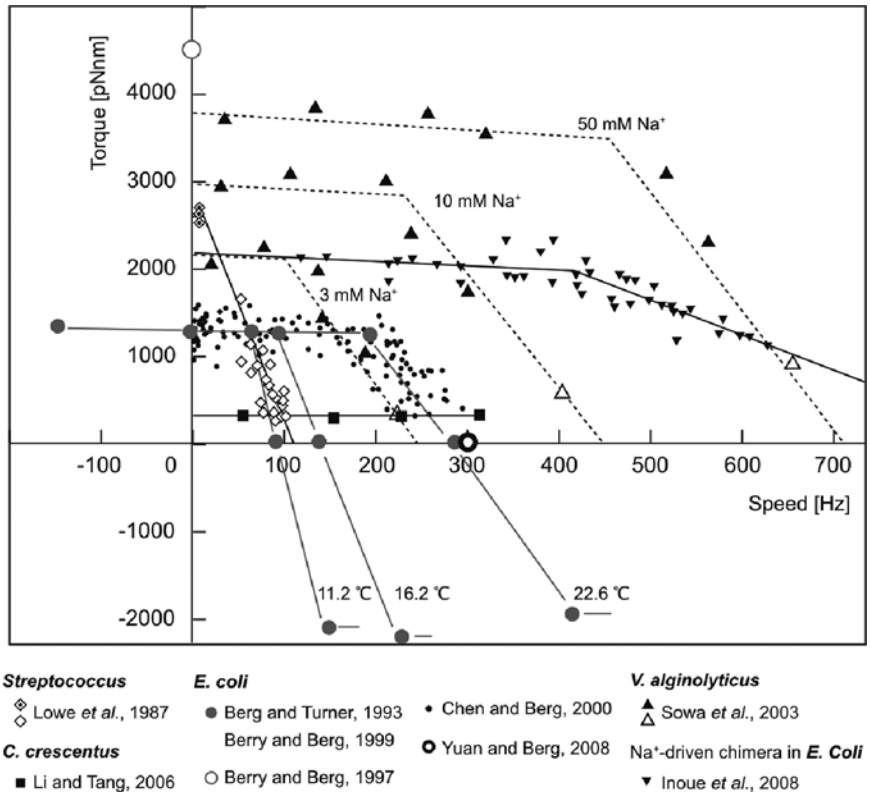

Figure 7.7. Torque–speed relationships for flagellar motors of various species with wild-type numbers of stator units. Upright triangles and dashed lines are data for the Na^+ motor of *Vibrio alginolyticus* at three different external Na^+ concentrations; inverted triangles and solid line are data for the Na^+-driven chimera in *Escherichia coli* at high sodium-motive force. The data for the H^+ motor of *E. coli* are all in agreement, except for the grey open circle at zero speed, which is probably too high due to systematic errors in the calibration of the optical trap. The low-speed data point for *Streptococcus* (*filled diamond*) may also be too high due to a systematic error. Except where indicated, all measurements were made at room temperature. For more details see references indicated in the legend. The *E. coli* experiments using electrorotation (*grey filled circles*) and beads (*black filled circles*) did not report absolute torques—these curves have been scaled to a stall torque of 1,260 pN nm (Reid et al. 2006). *C. crescentus*, *Caulobacter crescentus.*

constant (slowly declining) up to several 100 Hz. At higher speeds the motor torque declines more steeply and approximately linearly. The transition between these two limits has been called the "knee" and is temperature dependent. Torque–speed curves obtained by electrorotation are in agreement with those found by other methods and extend the measurements backwards to ∼100 Hz and forwards beyond the zero-load speed of the motor. The torque generated at high load is independent of temperature (Berg and Turner 1993, Chen and Berg 2000a), hydrogen isotope (Chen and Berg 2000b), and the composition of the IMF (Manson et al. 1980), consistent with tight coupling, constant efficiency, and mechanical rate limitation. By contrast, the torque at low load depends on all three factors (Chen and Berg 2000a, b), indicating rate-limiting kinetic steps such as ion binding and transit through the motor or conformational changes.

The most reliable estimate of the absolute magnitude of torque generated by the *E. coli* motor, 1,260 ± 190 pN nm rad^{-1}, comes from the measurements with polystyrene beads of diameter 1 μm (for which the uncertainty introduced by unknown filament lengths is negligible) (Reid et al. 2006). The torque in the chimeric motor is a little higher. As in F_o, conservation of energy sets a lower limit to the number of ions that must flow in the motor per revolution, $N_{min} = (2\pi M)/(q \cdot \text{IMF})$. For a single-stator chimeric motor at high SMF driving a 1-μm bead, $N_{min} = 36 \pm 6$ (Lo et al. 2007).

7.5. Mechanism

7.5.1. ATP-Synthase

F_1F_o

A substantial effort from several laboratories around the world has gone into investigating rotation powered by F_o on a single-molecule level. Because F_o is membrane bound and requires an energized membrane to work, these experiments are difficult, progress is slow, and experimental data are noisy. All attempts have used F_1F_o reconstituted into phospholipid vesicles. Coupled rotation of F_1F_o has been demonstrated using both polarization microscopy of single fluorophores (Figure 7.4F) and single-pair FRET (Figure 7.4G). The polarization experiment showed rotation of the enzyme during synthesis upon applying a diffusion potential but not with a Na^+ concentration gradient alone, and during hydrolysis but only in the presence of Na^+ (Kaim et al. 2002). Rotation was sensitive to *N*,*N*′- dicyclohexylcarbodiimide (DCCD), a known F_o rotation inhibitor, further confirming that F_o was indeed rotating. The frequency of observed oscillations in the polarization signal, corresponding to rotation, was consistent with expected rates for a given [ATP] based on previously observed F_1 rotation. The first FRET experiment (Figure 7.4G) showed three distinct FRET levels between fluorophores on the γ- and *b*-subunits that were consistent with 120° rotations of γ, and cycling between these levels during ATP hydrolysis (Borsch et al. 2002). Later work by the same group using similar methods showed cycling among the same three FRET levels but in opposite directions during hydrolysis and synthesis (Diez et al. 2004, Zimmermann et al. 2005) (Figure 7.8). The PMF for synthesis consisted of a K^+ diffusion potential plus a pH gradient; FRET was between an acceptor on the *b*-subunit and a donor on either the γ- or the ε-subunit. The later experiments also showed a breaking of the threefold symmetry of F_1, presumably due to interactions with the second stalk (*b*-subunits) and/or the fluorophores.

Stepping in F_1F_o is complicated by the different rotational symmetries of the two component motors. Whereas isolated F_o would be expected to take about ten steps per revolution, one per subunit of the C-ring, coupling of the C-ring to the F_1 rotor in F_1F_o is expected to introduce threefold symmetry to the rotation. Thus the number of steps observed is expected to vary from about ten if relative rotation of *c*- and *a*-subunits is measured to three if relative rotation of the rotor and stator of F_1 is measured. One possible explanation of the threefold stepping observed in the FRET experiments is that an elastic compliance between the F_1 and F_o rotors, or between the *b*- and *a*-subunits in F_o, filters out the F_o steps. Alternatively, even a perfect F_o FRET-label pair would be expected to show three steps at low time resolution if step times in F_o are not equally distributed but instead controlled by interaction with F_1. Thus the experiment would resolve only the dwell before a critical rate-limiting step in which ATP in synthesized, with all other F_o steps happening too fast to resolve. Single-pair FRET

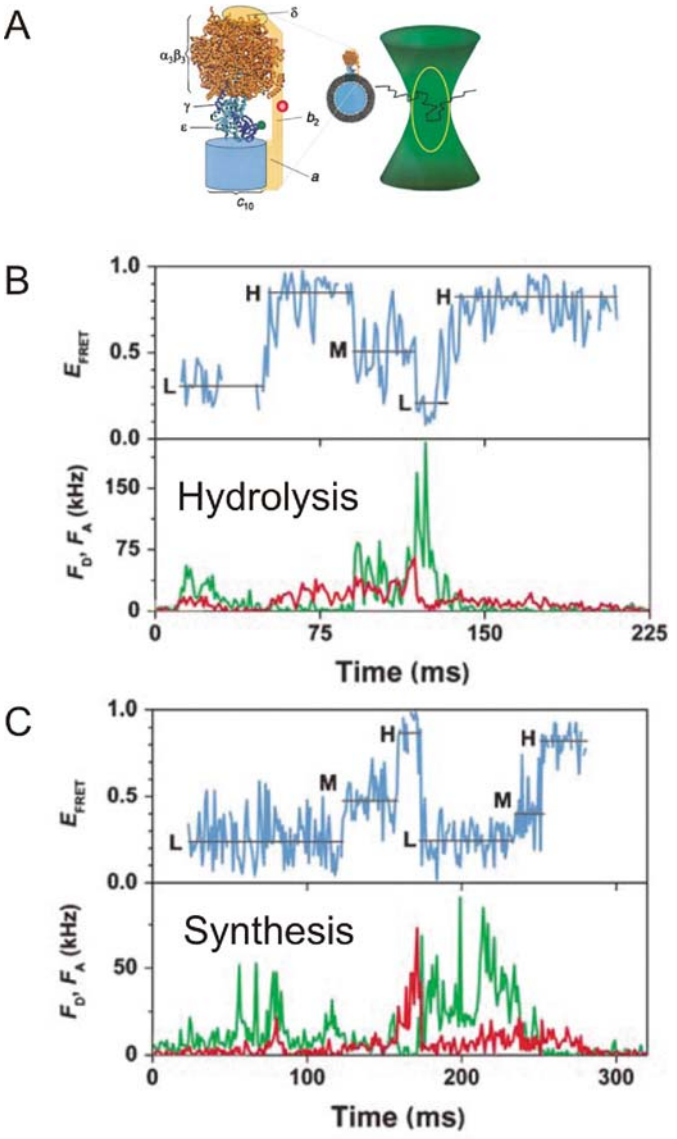

Figure 7.8. Detection of stepping rotation in F_1F_o using fluorescence resonance energy transfer (FRET) between fluorophores attached to the ε- and *b*-subunits. **A.** FRET-labelled F_1F_o is reconstituted into vesicles, which give bursts of photons each time they diffuse freely through a confocal laser excitation spot. The distance between fluorophores, and thus the FRET efficiency (E_{FRET}), cycles through three values, indicating 120° steps. The direction of cycling is opposite during adenosine triphosphate hydrolysis **(B)** and synthesis **(C)**. The lower plots in panels B and C show donor (*green*) and acceptor (*red*) fluorescence intensities. [From Zimmermann et al. (2005), with permission.]

is an ideal technique for probing this question because fluorophore pairs can in principle be engineered to monitor relative motions of different parts of the enzyme.

F_1

Compared to F_o and F_1F_o, single-molecule experiments on F_1 have been numerous and the data quality exceptionally high, allowing a detailed picture of the mechanism of F_1 to be built. The majority of the work has used TF_1, which has the advantages that it is probably more robust to denaturation and other mechanical damage and furthermore that at room temperature it is operating far below its normal temperature, resulting in slow kinetics that are an aid to direct detection with single-molecule methods. Unless otherwise stated, this section refers to TF_1. In 1998 the actin filament rotation assay revealed discrete 120° steps in F_1 rotation (Yasuda et al. 1998) in nanomolar [ATP]. The "transient" torque in discrete stepping traces was defined as $M = (2\pi/3)\zeta/\tau_{\text{step}}$, where τ_{step}, the time required to complete a step, was estimated by aligning many steps and averaging. The transient torque thus obtained was $\sim$40 pN nm rad^{-1}, similar to the average torque generated by F_1 driving a large viscous load. In 2000, stepping rotation was confirmed using angle-resolved single-fluorophore imaging, ruling out the possibility that interactions between the actin filament and F_1, rather than the mechanism of F_1, were responsible for the steps (Adachi et al. 2000).

Since 2001, polystyrene and gold nanoparticles with diameters ranging from 40 to 300 nm have been the label of choice for measuring F_1 rotation because their high light-scattering cross section and small size combine to give the best possible combination of time and angular resolution. The first experiment to use gold labels (Yasuda et al. 2001) allowed a detailed analysis of stepping rotation that gave a great insight into the mechanism of ATP hydrolysis by F_1. At high [ATP] only 120° steps were seen, whereas at low [ATP] substeps of 80° and 40° could be distinguished (Figure 7.9A). The initial report actually estimated 90° and 30° substeps. A later experiment using bead pairs rather than single beads to improve angular resolution gave improved estimates of 80° and 40° (Shimabukuro et al. 2003). To avoid confusion, we will use the later, improved estimates of 80° and 40° throughout this section. The duration of the 120° step at saturating [ATP] was roughly equal to that of the 40° substeps at low concentrations, indicating that the 80° substep becomes fast at high [ATP], but that the 40° substep is ATP independent. Because the 80° substep gets longer as [ATP] decreases, it is natural to assume that it corresponds to a step in which the ATP molecule binds to F_1. An analysis of the distribution of times taken to rotate 120° confirmed this. At low [ATP], ATP binding is rate limiting, and the 80° substep takes far longer than the 40° substep. Under these conditions the distributions were well fitted by a single exponential with a rate directly proportional to [ATP], giving a second-order rate constant $k_{\text{on}} = (3.0 \pm 0.1) \times 10^7$ M^{-1} sec^{-1} for ATP binding. At saturating [ATP] the 40° substep dominates, and distributions fitted a double-exponential with rates $k_1 = (1.64 \pm 0.06)$ msec^{-1} and $k_2 = (0.71 \pm 0.02)$ msec^{-1}, indicating that two sequential processes with approximately millisecond rates are required before a 40° substep. These results were consistent with the average rotation speeds and bulk ATP hydrolysis rates described in the subsection on F_1 in Section 7.4.1 and outlined the essential features of the catalytic cycle illustrated in Figure 7.9B.

In 2003, one of the two reactions in the 40° substep was identified as ATP cleavage, using a mutant that slowly hydrolyses ATP and a slowly hydrolysable substrate ATPγS (Shimabukuro et al. 2003). Further correspondence between chemical reactions and rotational

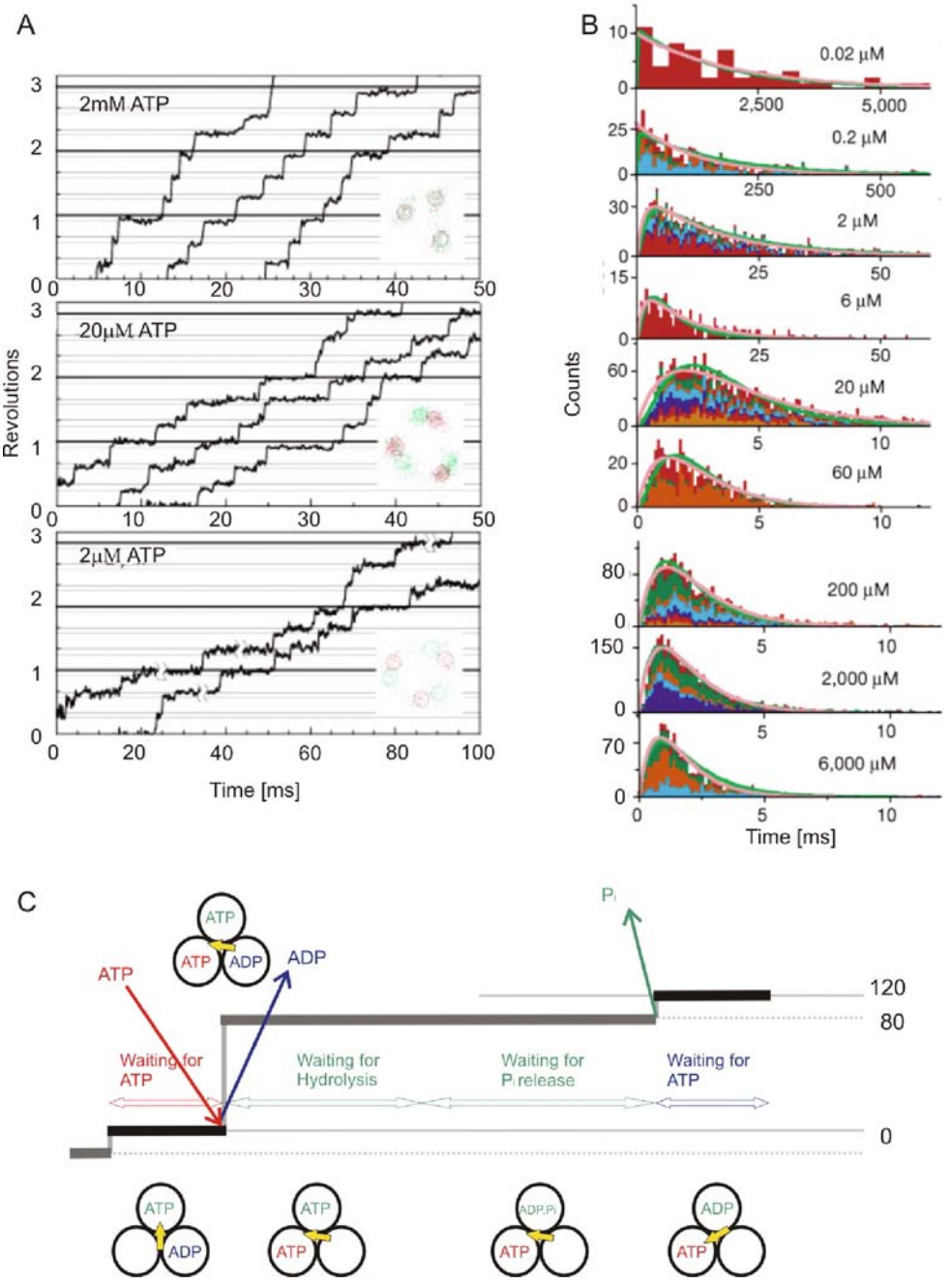

Figure 7.9. A. Angle versus time traces for single 40-nm gold beads attached to the γ-subunit of immobilized F_1, with three different adenosine triphosphate concentrations [ATP]. The larger substep is not resolved at the highest [ATP] **(panel)**. The insets show the traces of the bead positions from which angles were calculated. **B.** A schematic of the mechanochemical cycle of F_1. The inorganic phosphate (P_i) release from the most recently hydrolysed ATP molecule is shown as the trigger of the smaller substep, although it is also possible that each P_i is retained for a further 120°. ADP, adenosine diphosphate. [Panel A, from Yasuda et al. (2001), with permission. Panel C, adapted from Adachi et al. (2007).]

steps was investigated in 2004 by simultaneous observation of the binding of fluorescently labelled ATP and the rotation of bead pairs (Nishizaka et al. 2004). It was found that (1) ATP (or ADP) stays bound to the F_1 during two 120° steps, (2) the 80° substep happens immediately after the fluorescently labelled ATP binds to the motor, and (3) the bead angle and polarization of the fluorescent dye molecule were correlated, implying that the orientation of the γ-subunit dictates which β-subunit will bind the next ATP. In 2007 further observation of fluorescently labelled ATP with a total internal reflection fluorescence microscope (TIRFM) revealed that ADP is released during the 80° substep after it has been bound for two 120° steps, not, for example, during the last 40° substep of the two 120° steps during which it stays bound (Adachi et al. 2007). These results were also taken as an indication that the affinity of ADP decreases with rotation and that the ADP release contributes in energy to the 80° rotation induced by the ATP binding (Adachi et al. 2007). In addition, by adding 200–500 mM [P_i] to the TF_1 rotation observation chamber, the experiments of 2007 observed an increased in dwell time after the 80° substep and thus identifying the second of the two ∼1-ms reactions in the 40° substep with P_i release (Adachi et al. 2007). In terms of site occupancy, two of the three catalytic sites were occupied at high [ATP], whereas at lower [ATP] a variety of irregular behaviours was observed, most likely representing nonmajor reaction pathways (Adachi et al. 2007). The current best estimate of the mechanochemical coupling scheme in which all three of the β-subunits participate in one 120° step (Ariga et al. 2007) is given in Figure 7.9C (Adachi et al. 2007). One open question is whether P_i is released immediately after ATP hydrolysis, as illustrated in Figure 7.9C, or stays bound for an extra 120° step (Adachi et al. 2007).

The following conclusions were drawn from measurements of average and transient torque: (1) The so-called "DELSEED" region, a conserved acidic region on the β-subunit in contact with the γ-subunit, does not have a direct role (Hara et al. 2000). (2) Torque generated by mutants with one, two, or three altered catalytic sites that bind ATP slowly is unchanged, despite the fact that the binding affinity (k_{on} rate) is reduced (Ariga et al. 2002). The torque generated by the wild-type F_1 when using other nucleotide triphosphates whose k_{on} rate is lower than that of ATP was also unchanged (Noji et al. 2001). This can be explained with the "binding zipper" model proposed by Oster and Wang (2000), which divides the ATP-binding process into docking of ATP (described by k_{on}) and the torque generation as a result of the zipping of hydrogen bounds between the P_i moiety of ATP and residues of the catalytic site. (3) The rotor tip inside the $\alpha_3\beta_3$ hexamer of TF_1 is not strictly necessary for torque generation (Hossain et al. 2006, Iwamoto et al. 1990, Sokolov et al. 1999, Müller et al. 2002). Recently the role of the rotor shaft in the generation of torque was investigated further (Furuike et al. 2008). In 2008 the rotor tip placed inside of the stator hexamer was truncated up to the point where what remained of the γ-subunit was almost all outside the stator cavity. All of the mutants rotated in the right direction, with lower speeds and increasingly irregular motion observed as the γ-subunit was shortened (Furuike et al. 2008). It seems that the top surface of the $\alpha_3\beta_3$ hexamer provides the interactions with γ required to produce torque, and the fixed pivot and rigid axle are not needed but stabilize the torque generation, making if more effective. However, the speed of rotation in the truncated mutants was the same as would be predicted from the ATP hydrolysis rate of F_1 lacking the γ-subunit, indicating that care should be taken in interpreting these results. Perhaps the truncated γ-subunit merely reports the intrinsic residual activity of the $\alpha_3\beta_3$ hexamer rather than retaining any of its natural coordinating function.

7.5.2. Bacterial Flagellar Motor

Independent Torque-Generating Units

Proton flux in the bacterial flagellar motor passes through torque-generating stator units, probably consisting of four MotB and two MotA proteins (Sato and Homma 2000, Yorimitsu et al. 2004). Early studies showed that *mot* mutants of *E. coli* do not rotate (Armstrong and Adler 1969) but can be "resurrected" through protein synthesis by lambda-transducing phages (Silverman et al. 1976). This resurrection has also been studied on the level of single motors. Cells of a *motB* strain carrying plasmids with wild-type *motB* genes controlled by the *lac* promoter, as well as cells with *motA* and *motB* point and deletion mutations carrying plasmids with wild-type *motA* and *motB* genes, were tethered to the surface and resurrected. Stepwise increments in motor speed rotation were observed after addition of the inducer, showing that bacterial flagellar motors contain several independent torque-generating units (Block and Berg 1984, Blair and Berg 1988). The maximum number of speed increments observed in these early experiments was 8 (Blair and Berg 1988). More recently, using polystyrene beads attached to the sheared filaments of *E. coli* wild-type and Na^+-driven chimeric motors, the number of discrete steps observed has increased to at least 11 (Reid et al. 2006). Stepwise decreases in motor rotation speed upon activation of an irreversible Na^+-channel inhibitor were observed in Na^+-driven alkalophilic *Bacillus* as well, indicating that this species has up to 9 independent stator units (Muramoto et al. 1994). Transient speed changes observed in wild-type motor rotation suggested the possibility that the units are not fixed but in a process of constant turnover (Reid et al. 2006). This was confirmed in 2006 by observing green-fluorescent protein (GFP)–labelled MotB in live cells, using TIRFM (Leake et al. 2006). Motors were seen as bright spots, which were estimated by quantitative photobleaching to contain an average of ~22 GFP molecules, consistent with the previous estimate of at least 11 units each containing two copies of MotB. A freely diffusing pool of ~200 GFP-MotB molecules was observed in the cell membrane, and the exchange between the pool and stator units within the motor on a timescale of minutes was demonstrated using fluorescence recovery after photobleaching (Leake et al. 2006).

Motor speed is proportional to the number of units in the high-load regime. A slight reduction in the speed per unit at higher number was seen for H^+- but not for Na^+-driven motors (Reid et al. 2006). This is attributed either to steric hindrance once a large number of units is present or possibly to local depletion of H^+ ions. Torque–speed curves for fully energized H^+ motors containing small numbers of units have been obtained using polystyrene beads 0.3–1.0 μm in diameter attached to flagellar stubs (Ryu et al. 2000) and 60-nm gold beads attached to hooks (Yuan and Berg 2008). The experiments with polystyrene beads showed that the torque generated at a given speed by a motor with N units is simply N times the torque generated by a single unit at that speed. This means that one unit rotates the motor as fast as many as the load tends to zero, a prediction that was confirmed by the gold bead experiment: Under experimental conditions that gave stepwise resurrection with larger loads, gold beads showed only sudden jumps from 0 Hz to the zero-load speed of ~300 Hz. These results can be reproduced by a model in which the duty ratio of each unit is high—that is, it seldom if ever detaches from the rotor—and in which the rate-limiting step at low load is insensitive to the torque exerted upon one unit by the action of other units upon the rotor (Ryu et al. 2000).

Interactions between Rotor and Stator

By combining atomic structures of fragments of the rotor proteins FliG, FliM, and FliN with cross-linking and mutational studies, the following picture of rotor–stator interactions involved in torque generation has emerged. Stator proteins form ion channels, with a single

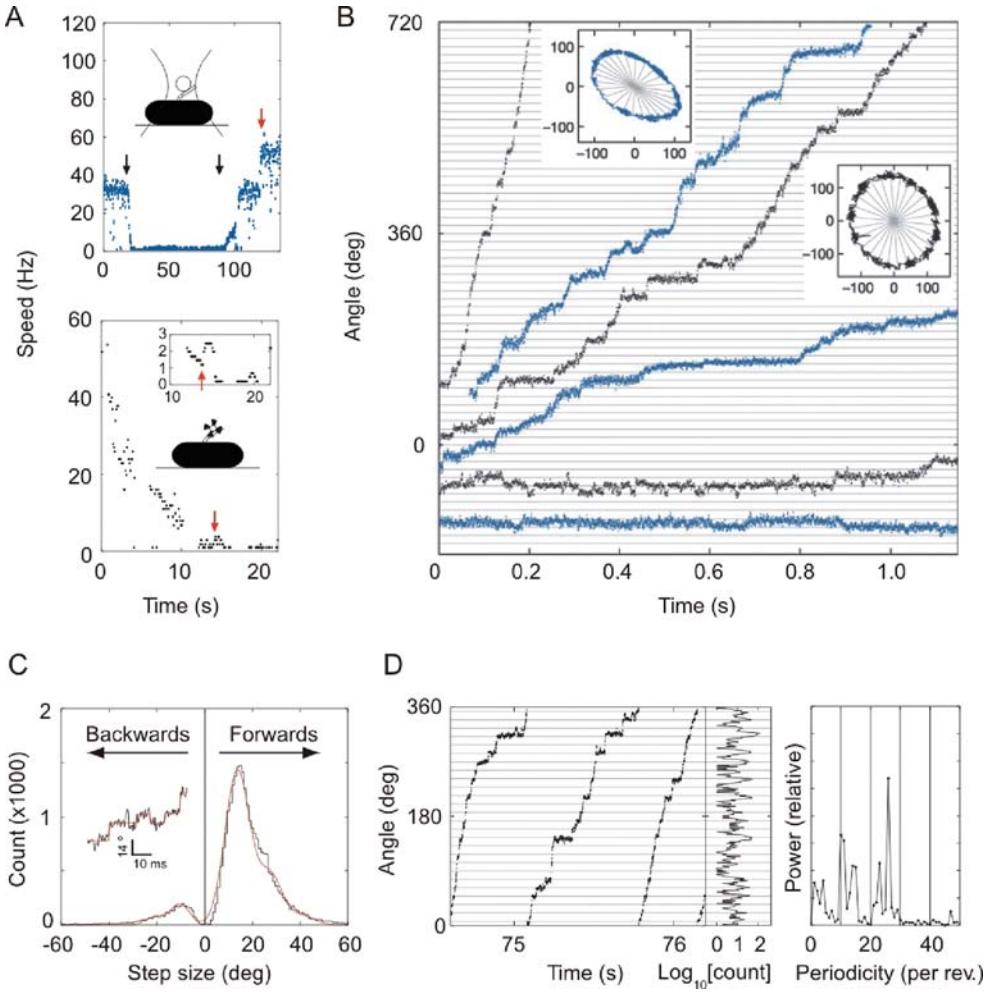

Figure 7.10. Steps in slow flagellar rotation. **A.** Reducing sodium-motive force (SMF) and motor speed of a chimeric Na^+-driven flagellar motor in *Escherichia coli* **(upper)** by lowering the external Na^+ concentration (from 5 mM to 0.1 mM and back; *black arrows*) and **(lower)** by photodamage. The speed doublings marked by red arrows indicate a probable change from one to two stators. **B.** Stepping rotation of flagellar motors with a range of average speeds depending on different SMF. Insets show the positions of beads attached to flagellar filaments; scales are in nanometres. Horizontal and radial lines indicate 1/26 revolution. **C.** Step-size distribution (*black*) with multiple Gaussian fit (*red*). The peak of forwards steps is 13.7°, indicating 26 steps per revolution. An example of steps identified by a step-finding algorithm is shown in the inset. **D.** Plot of angle against time during three revolutions, a histogram of dwell angles for the same revolutions, and the power spectrum of that histogram. The peak at 26 per revolution corresponds to a step size of 13.8° and shows that the motor stops at the same angles on successive revolutions. Speeds shown in black were measured using optical interferometry, those in blue using high-speed fluorescence microscopy (insets in panel A). [Adapted from Sowa et al. (2005).]

essential conserved acidic residue in MotB (Asp32 in *E. coli*) identified as the key ion-binding site (Sharp et al. 1995a, b). Five charged residues in the C-terminal domain of FliG interact with two charged residues in the cytoplasmic domain of MotA (Lloyd and Blair 1997, Zhou and Blair 1997, Zhou et al. 1998a) to generate torque. FliG and PomA in the Na^+-driven motor of *V. alginolyticus* interact via different charged residues but in a similar pattern (Yakushi et al. 2006, Yorimitsu et al. 2002, 2003). Single mutations of any of these residues reduce but do not abolish rotation, and charge-reversing second mutations can reverse the effect of single mutations. Therefore FliG–MotA interaction during torque generation is probably an electrostatic interaction between extended parts of the two proteins. The interaction is thought to be driven by Asp32 of MotB accepting an ion and inducing conformational changes in MotA (Braun et al. 1999, Kojima and Blair 2001).

Stepping Rotation

Unlike F_1 and several other ATP-driven motors discussed in this book, direct observation of steps corresponding to single mechanochemical cycles of the BFM has been limited by the high speed and small step size of the motor. Analysis of speed fluctuations of motors with different numbers of torque-generating units, combined with electrorotation and measurements with broken motors, demonstrated that the BFM is a stepping motor rather than a "fluid drive" (Samuel and Berg 1995, 1996). Assuming Poisson statistics for steps led to an estimate of ~50 steps per unit per revolution. The proportionality between step number and unit number is consistent with a high duty ratio. It should be noted, however, that the "steps" here need not correspond to actual physical movements of the rotor; rather they are strictly defined as "independent sequential stochastic events." Just as the passage of several ions in F_o might be stored up to produce a single observable 120° step in F_1F_o, so might the events identified by the fluctuation analysis be linked only indirectly to observable steps.

Such steps were first observed in 2005 in a Na^+-driven chimeric flagellar motor in *E. coli* (Sowa et al. 2005). At low sodium motive force and with controlled expression of a small number of torque-generating units, 26 steps per revolution were seen (Figure 7.10). This identifies the inner lobe of the C-ring as the site of stepping and thus presumably of torque generation. However, many questions remain unanswered. It has proved difficult to reconcile 26 steps per revolution with the estimate of 36 ± 6 ions per stator per revolution estimated from the energetics of flagellar rotation in the chimeric motor and the assumption that each step should correspond to an integer number of ions crossing the membrane. Future investigations of stepping under well-controlled conditions of known SMF and number of stator units will be necessary to reveal the details of the mechanism of the BFM in the way that measurements of steps and substeps have done for F_1.

References

Abrahams JP, Leslie AG, Lutter R, Walker JE (1994) Structure at 2.8 A resolution of F_1-ATPase from bovine heart mitochondria. Nature 370: 621–628.

Adachi K, Yasuda R, Noji H, Itoh H, Harada Y, Yoshida M, Kinosita K (2000) Stepping rotation of F_1-ATPase visualized through angle-resolved single-fluorophore imaging. Proc Natl Acad Sci USA 97: 7243–7247.

Adachi K, Oiwa K, Nishizaka T, Furuike S, Noji H, Itoh H, Yoshida M, Kinosita K (2007) Coupling of rotation and catalysis in F(1)-ATPase revealed by single-molecule imaging and manipulation. Cell 130: 309–321.

Aizawa SI (1996) Flagellar assembly in *Salmonella typhimurium*. Mol Microbiol 19: 1–5.

Althoff G, Lill H, Junge W (1989) Proton channel of the chloroplast ATP synthase, CF_0: its time-averaged single-channel conductance as function of pH, temperature, isotopic and ionic medium composition. J Membr Biol 108: 263–271.

Arai H, Terres G, Pink S, Forgac M (1988) Topography and subunit stoichiometry of the coated vesicle proton pump. J Biol Chem 263: 8796–8802.

Ariga T, Masaike T, Noji H, Yoshida M (2002) Stepping rotation of F(1)-ATPase with one, two, or three altered catalytic sites that bind ATP only slowly. J Biol Chem 277: 24870–24874.

Ariga T, Muneyuki E, Yoshida M (2007) F_1-ATPase rotates by an asymmetric, sequential mechanism using all three catalytic subunits. Nat Struct Mol Biol 14: 841–846.

Armstrong JB, Adler J (1969) Complementation of nonchemotactic mutants of *Escherichia coli*. Genetics 61: 61–66.

Asai Y, Yakushi T, Kawagishi I, Homma M (2003) Ion-coupling determinants of Na+-driven and H+-driven flagellar motors. J Mol Biol 327: 453–463.

Baker MD, Wolanin PM, Stock JB (2006) Signal transduction in bacterial chemotaxis. Bioessays 28: 9–22.

Berg HC, Anderson RA (1973) Bacteria swim by rotating their flagellar filaments. Nature 245: 380–382.

Berg HC, Turner L (1993) Torque generated by the flagellar motor of *Escherichia coli*. Biophys J 65: 2201–2216.

Berg HC (2003) The rotary motor of bacterial flagella. Annu Rev Biochem 72: 19–54.

Berg JM, Tymoczko JL, Stryer L (2002) *Biochemistry*. WH Freeman, New York.

Berry RM, Berg HC (1996) Torque generated by the bacterial flagellar motor close to stall. Biophys J 71: 3501–3510.

Berry RM, Berg HC (1997) Absence of a barrier to backwards rotation of the bacterial flagellar motor demonstrated with optical tweezers. Proc Natl Acad Sci USA 94: 14433–14437.

Berry RM, Berg HC (1999) Torque generated by the flagellar motor of *Escherichia coli* while driven backward. Biophys J 76: 580–587.

Berry RM, Turner L, Berg HC (1995) Mechanical limits of bacterial flagellar motors probed by electrorotation. Biophys J 69: 280–286.

Beyenbach KW, Wieczorek H (2006) The V-type H+ ATPase: molecular structure and function, physiological roles and regulation. J Exp Biol 209: 577–589.

Blair DF, Berg HC (1988) Restoration of torque in defective flagellar motors. Science 242: 1678–1681.

Blair DF (1995) How bacteria sense and swim. Annu Rev Microbiol 49: 489–522.

Blair DF, Berg HC (1991) Mutations in the MotA protein of *Escherichia coli* reveal domains critical for proton conduction. J Mol Biol 173: 4049–4055.

Block SM, Berg HC (1984) Successive incorporation of force-generating units in the bacterial rotary motor. Nature 309: 470–472.

Block SM, Blair DF, Berg HC (1989) Compliance of bacterial flagella measured with optical tweezers. Nature 338: 514–518.

Block SM, Fahrner KA, Berg HC (1991) Visualization of bacterial flagella by video-enhanced light microscopy. J Bacteriol 173: 933–936.

Borsch M, Diez M, Zimmermann B, Reutera R, Graber P (2002) Stepwise rotation of the γ-subunit of EF_0F_1-ATP synthase observed by intramolecular single-molecule fluorescence resonance energy transfer. FEBS Lett 527: 147–152.

Bowler MW, Montgomery MG, Leslie AG, Walker JE (2007) Ground state structure of F1-ATPase from bovine heart mitochondria at 1.9 A resolution. J Biol Chem 282: 14238–14242.

Boyer PD (1993) The binding change mechanism for ATP synthase-some probabilities and possibilities. Biochim Biophys Acta 1140: 215–250.

Braun TF, Poulson S, Gully JB, Empey JC, Van Way S, Putnam A, Blair DF (1999) Function of proline residues of MotA in torque generation by the flagellar motor of *Escherichia coli.* J Bacteriol 181: 3542–3551.

Brown PN, Hill CP, Blair DF (2002) Crystal structure of the middle and C-terminal domains of the flagellar rotor protein FliG. EMBO J 21: 3225–3234.

Brown PN, Mathews MA, Joss LA, Hill CP, Blair DF (2005) Crystal structure of the flagellar rotor protein FliN from *Thermotoga maritime*. J Bacteriol 187: 2890–2902.

Brown PN, Terrazas M, Paul K, Blair DF (2007) Mutational analysis of the flagellar protein FliG: sites of interaction with FliM and implications for organization of the switch complex. J Bacteriol 189: 305–312.

Chen X, Berg HC (2000a) Torque-speed relationship of the flagellar rotary motor of *Escherichia coli*. Biophys J 78: 1036–1041.

Chen X, Berg HC (2000b). Solvent-isotope and pH effects on flagellar rotation in *Escherichia coli*. Biophys J 78: 2280–2284.

Cherepanov DA, Junge W (2001) Viscoelastic dynamics of actin filaments coupled to rotary F-ATPase: curvature as an indicator of the torque. Biophys J 81: 1234–1244.

Chernyak BV, Glagolev AN, Sherman MY, Skulachev VP (1983) A novel type of energetics in a marine alkalitolerant bacterium. DmNa-driven motility and sodium cycle. FEBS Lett 164: 38–42.

Chun SY, Parkinson JS (1988) Bacterial motility: membrane topology of the *Escherichia coli* MotB protein. Science 239: 276–278.

Darnton NC, Berg HC (2007) Force-extension measurements on bacterial flagella: triggering polymorphic transformations. Biophys. J 92(6): 2230–2236.

Darnton NC, Turner L, Rojevsky S, Berg HC (2007) On torque and tumbling in swimming *Escherichia coli*. J Bacteriol 189: 1756–1764.

Diez M, Zimmermann B, Börsch M, König M, Schweinberger E, Steigmiller S, Reuter R, Felekyan S, Kudryavtsev V, Seidel CA, Gräber P (2004) Proton powered subunit rotation in single membrane-bound F_0F_1-ATP synthase. Nat Struct Mol Biol 11: 135–141.

Duncan TM, Bulygin VV, Zhou Y, Hutcheon ML, Cross RL (1995) Rotation of subunits during catalysis by *Escherichia coli* F1-ATPase. Proc Natl Acad Sci USA 92: 10964–10968.

Falke JJ, Bass RB, Butler SL, Chervitz SA, Danielson MA (1997) The two-component signaling pathway of bacterial chemotaxis: a molecular view of signal transduction by receptors, kinases, and adaptation enzymes. Annu Rev Cell Dev Biol 13: 457–512.

Felle H, Porter JS, Slayman CL, Kaback HR (1980) Quantitative measurements of membrane potential in *Escherichia coli*. Biochemistry 19: 3585–3590.

Feniouk BA, Cherepanov DA, Junge W, Mulkidjanian AY (2001) Coupling of proton flow to ATP synthesis in *Rhodobacter capsula*tus: F(0)F(1)-ATP synthase is absent from about half of chromatophores. Biochim Biophys Acta 1506: 189–203.

Feniouk BA, Cherepanov DA, Voskoboynikova NE, Mulkidjanian AY, Junge W (2002) Chromatophore vesicles of *Rhodobacter capsulatus* contain on average one F(0)F(1)-ATP synthase each. Biophys J 82: 1115–1122.

Feniouk BA, Kozlova MA, Knorre DA, Cherepanov DA, Mulkidjanian AY, Junge W (2004) The proton driven rotor of ATP synthase: ohmic conductance (10 fS), and absence of voltage gating. Biophys J 86: 4094–4109.

Friedl P, Schairer HU (1981) The isolated F_0 of *Escherichia coli* ATP-synthase is reconstitutively active in H+-conduction and ATP-dependent energy-transduction. FEBS Lett 128: 261–264.

Fritz M, Klyszejko AL, Morgner N, Vonck J, Brutschy B, Muller DJ, Meier T, Müller V (2008) An intermediate step in the evolution of ATPases—a hybrid Fo–Vo rotor in a bacterial Na+ F1F0 ATP synthase. FEBS J 275: 1999–2007.

Fung DC, Berg HC (1995) Powering the flagellar motor of *Escherichia coli* with an external voltage source. Nature 375: 809–812.

Furuike S, Hossain MD, Maki Y, Adachi K, Suzuki T, Kohori A, Itoh H, Yoshida M, Kinosita K (2008) Axle-less F1-ATPase rotates in the correct direction. Science 319: 955–958.

Gabel CV, Berg HC (2003) The speed of the flagellar rotary motor of *Escherichia coli* varies linearly with protonmotive force. Proc Natl Acad Sci USA 100: 8748–8751.

Gibbons C, Montgomery MG, Leslie AG, Walker JE (2000) The structure of the central stalk in bovine F_1-ATPase at 2.4 A resolution. Nat Struct Biol 7: 1055–1061.

Hara KY, Noji H, Bald D, Yasuda R, Kinosita K, Yoshida M (2000) The role of the DELSEED motif of the beta subunit in rotation of F1-ATPase. J Biol Chem 275: 14260–14263.

Hirono-Hara Y, Noji H, Nishiura M, Muneyuki E, Hara KY, Yasuda R, Kinosita K, Yoshida M (2001) Pause and rotation of F(1)-ATPase during catalysis. Proc Natl Acad Sci USA 98: 13649–13654.

Hirono-Hara Y, Ishizuka K, Kinosita K, Yoshida M, Noji H (2005) Activation of pausing F_1 motor by external force. Proc Natl Acad Sci USA 102: 4288–4293.

Hirota N, Kitada M, Imae Y (1981) Flagellar motors of alkalophilic *Bacillus* are powered by an electrochemical potential gradient of Na^+. FEBS Lett 132: 278–280.

Hirota N, Imae Y (1983) Na+-driven flagellar motors of an alkalophilic *Bacillus* strain YN-1. J Biol Chem 258: 10577–10581.

Holzenburg A, Jones PC, Franklin T, Pali T, Heimburg T, Marsh D, Findlay JB, Finbow ME (1993) Evidence for a common structure for a class of membrane channels. Eur J Biochem 213: 21–30.

Hossain MD, Furuike S, Maki Y, Adachi K, Ali MY, Huq M, Itoh H, Yoshida M, Kinosita K (2006) The rotor tip inside a bearing of a thermophilic F_1-ATPase is dispensable for torque generation. Biophys J 90: 4195–4203.

Hotani H (1976) Light microscope study of mixed helices in reconstituted *Salmonella* flagella. J Mol Biol 106: 151–166.

Hudson GS, Mason JG, Holton TA, Koller B, Cox GB, Whitfeld PR, Bottomley W (1987) A gene cluster in the spinach and pea chloroplast genomes encoding one CF1 and three CF0 subunits of the H^+-ATP synthase complex and the ribosomal protein S2. J Mol Biol 196: 283–298.

Iko Y, Sambongi Y, Tanabe M, Iwamoto-Kihara A, Saito K, Ueda I, Wada Y, Futai M (2001) ATP synthase F_1 sector rotation. Defective torque generation in the beta subunit Ser-174 to Phe mutant and its suppression by second mutations. J Biol Chem 276: 47508–47511.

Inoue Y, Lo CJ, Fukuoka H, Takahashi H, Sowa Y, Pilizota T, Wadhams GH, Homma M, Berry RM, Ishijima A (2008) Torque–speed relationships of Na+-driven chimeric flagellar motors in *Escherichia coli*. J Mol Biol 376: 1251–1259.

Irikura VM, Kihara M, Yamaguchi S, Sockett H, Macnab RM (1993) *Salmonella typhimurium* fliG and fliN mutations causing defects in assembly, rotation, and switching of the flagellar motor. J Bacteriol 175: 802–810.

Itoh H, Takahashi A, Adachi K, Noji H, Yasuda R, Yoshida M, Kinosita K (2004) Mechanically driven ATP synthesis by F_1-ATPase. Nature 427: 465–468.

Iwamoto A, Miki J, Maeda M, Futai M (1990) H(+)-ATPase gamma subunit of *Escherichia coli*. Role of the conserved carboxyl-terminal region. J Biol Chem 265: 5043–5048.

Jagendorf AT, Uribe E (1966) ATP formation caused by acid-base transition of spinach chloroplasts. Proc Natl Acad Sci USA 55: 170–177.

Junge W, Pänke O, Cherepanov DA, Gumbiowski K, Müller M, Engelbrecht S (2001) Inter-subunit rotation and elastic power transmission in F0F1-ATPase. FEBS Lett 504: 152–160.

Kaim G, Prummer M, Sick B, Zumofen G, Renn A, Wild UP, Dimroth P (2002) Coupled rotation within single F0F1 enzyme complexes during ATP synthesis or hydrolysis. FEBS Lett 525: 156–163.

Kanazawa H, Mabuchi K, Kayano T, Noumi T, Sekiya T, Futai M (1981) Nucleotide sequence of the genes for F0 components of the proton-translocating ATPase from *Escherichia coli*: prediction of the primary structure of F_0 subunits. Biochem Biophys Res Commun 103: 604–612.

Kashket ER, Blanchard AG, Metzger WC (1980) Proton motive force during growth of *Streptococcus lactis* cells. J Bacteriol 143: 128–134.

Kato-Yamada Y, Noji H, Yasuda R, Kinosita K, Yoshida M (1998) Direct observation of the rotation of epsilon subunit in F_1-ATPase. J Biol Chem 273: 19375–19377.

Khan S, Meister M, Berg HC (1985) Constraints on flagellar rotation. J Mol Biol 184: 645–656.

Kihara M, Miller GU, Macnab RM (2000) Deletion analysis of the flagellar switch protein FliG of *Salmonella*. J Bacteriol 182: 3022–3028.

Kojima S, Blair DF (2001) Conformational change in the stator of the bacterial flagellar motor. Biochemistry 40: 13041–13050.

Kudo S, Magariyama Y, Aizawa S (1990) Abrupt changes in flagellar rotation observed by laser dark-field microscopy. Nature 346: 677–680.

Larsen SH, Adler J, Gargus JJ, Hogg RW (1974) Chemomechanical coupling without ATP: the source of energy for motility and chemotaxis in bacteria. Proc Natl Acad Sci USA 71: 1239–1243.

Leake MC, Chandler JH, Wadhams GH, Bai F, Berry RM, Armitage JP (2006) Stoichiometry and turnover in single, functioning membrane protein complexes. Nature 443: 355–358.

Lill H, Engelbrecht S, Schönknecht G, Junge W (1986) The proton channel, CF0, in thylakoid membranes. Only a low proportion of CF_1-lacking CF_0 is active with a high unit conductance (169 fS). Eur J Biochem 160: 627–634.

Lloyd SA, Tang H, Wang X, Billings S, Blair DF (1996) Torque generation in the flagellar motor of *Escherichia coli*: evidence of a direct role for FliG but not for FliM or FliN. J Bacteriol 178: 223–231.

Lloyd SA, Blair DF (1997) Charged residues of the rotor protein FliG essential for torque generation in the flagellar motor of *Escherichia coli*. J Mol Biol 266: 733–744.

Lloyd SA, Whitbey FG, Blair DF, Hill CP (1999) Structure of the C-terminal domain of FliG, a component of the rotor in the bacterial flagellar motor. Nature 400: 472–475.

Lo CJ, Leake MC, Berry RM (2006) Fluorescence measurement of intracellular sodium concentration in single *Escherichia coli* cells. Biophys J 90: 357–365.

Lo CJ, Leake MC, Pilizota T, Berry RM (2007) Nonequivalence of membrane voltage and ion-gradient as driving forces for the bacterial flagellar motor at low load. Biophys J 93: 294–302.

Lowe G, Meister M, Berg HC (1987) Rapid rotation of flagellar bundles in swimming bacteria. Nature 325: 637–640.

Macnab RM (1976) Examination of bacterial flagellation by dark-field microscopy. J Clin Microbiol 4: 258–265.

Macnab RM (2003) How bacteria assemble flagella. Annu Rev Biochem 57: 77–100.

Magariyama Y, Susgiyama S, Muramoto K, Maekawa Y, Kawagishi I, Imae Y, Kudo S (1994) Very fast flagellar rotation. Nature 371: 752.

Manson MD, Tedesco P, Berg HC, Harold FM, Van Der Drift C (1977) A protonmotive force drives bacterial flagella. Proc Natl Acad Sci USA 74: 3060–3064.

Manson MD, Tedesco PM, Berg HC (1980) Energetics of flagellar rotation in bacteria. J Mol Biol 138: 541–561.

Matsuura S, Shioi J, Imae Y (1977) Motility in *Bacillus subtilis* driven by an artificial protonmotive force. FEBS Lett 82: 187–190.

Meier T, Matthey U, von Ballmoos C, Vonck J, Krug von Nidda T, Kühlbrandt W, Dimroth P (2003) Evidence for structural integrity in the undecameric *c*-rings isolated from sodium ATP synthases. J Mol Biol 325: 389–397.

Meier T, Polzer P, Diederichs K, Welte W, Dimroth P (2005) Structure of the rotor ring of F-type Na+-ATPase from *Ilyobacter tartaricus*. Science 308: 659–662.

Meister M, Berg HC (1987) The stall torque of the bacterial flagellar motor. Biophys J 52: 413–419.

Menz RI, Walker JE, Leslie AG (2001) Structure of bovine mitochondrial F_1-ATPase with nucleotide bound to all three catalytic sites: implications for the mechanism of rotary catalysis. Cell 106: 331–341.

Meyer Zu Tittingdorf JM, Rexroth S, Schäfer E, Schlichting R, Giersch C, Dencher NA, Seelert H (2004) The stoichiometry of the chloroplast ATP synthase oligomer III in *Chlamydomonas reinhardtii* is not affected by the metabolic state. Biochim Biophys Acta 1659:92–99.

Mitchell P (1961) Coupling of phosphorylation to electron and hydrogen transfer by a chemi-osmotic type of mechanism. Nature 191: 144–148.

Mitchell P (1966) Chemiosmotic coupling in oxidative and photosynthetic phosphorylation. Biol Rev Camb Philos Soc 1966 41: 445–502.

Mitome N, Ono S, Suzuki T, Shimabukuro K, Muneyuki E, Yoshida M (2002) The presence of phosphate at a catalytic site suppresses the formation of the MgADP-inhibited form of F_1-ATPase. Eur J Biochem 269: 53–60.

de Mot R, Vanderleyden J (1994) A conserved surface-exposed domain in major outer membrane proteins of pathogenic *Pseudomonas* and *Branhamella* species shares sequence homology with the calcium-binding repeats of the eukaryotic extracellular matrix protein thrombospondin. Mol Microbiol 13: 379–380.

Müller M, Pänke O, Junge W, Engelbrecht S (2002) F_1-ATPase, the C-terminal end of subunit gamma is not required for ATP hydrolysis-driven rotation. J Biol Chem 277: 23308–23313.

Muramoto K, Sugiyama S, Cragoe EJ, Imae Y (1994) Successive inactivation of the force-generating units of sodium-driven bacterial flagellar motors by a photoreactive amiloride analog. J Biol Chem 269: 3374–3380.

Muramoto K, Kawagishi I, Kudo S, Magariyama Y, Imae Y, Homma M (1995) High-speed rotation and speed stability of the sodium-driven flagellar motor in *Vibrio alginolyticus*. J Mol Biol 251: 50–58.

Murata T, Yamato I, Kakinuma Y, Leslie AG, Walker JE (2005) Structure of the rotor of the V-Type Na+-ATPase from *Enterococcus hirae*. Science 308: 654–659.

Murphy GE, Leadbetter JR, Jensen GJ (2006) *In situ* structure of the complete *Treponema primitia* flagellar motor. Nature 442: 1062–1064.

Nakanishi-Matsui M, Kashiwagi S, Hosokawa H, Cipriano DJ, Dunn SD, Wada Y, Futai M (2006) Stochastic high-speed rotation of *Escherichia coli* ATP synthase F_1 sector: the epsilon subunit-sensitive rotation. J Biol Chem 281: 4126–4131.

Nakanishi-Matsui M, Kashiwagi S, Ubukata T, Iwamoto-Kihara A, Wada Y, Futai M (2007) Rotational catalysis of *Escherichia coli* ATP synthase F_1 sector. Stochastic fluctuation and a key domain of the beta subunit. J Biol Chem 282: 20698–20704.

Negrin RS, Foster DL, Fillingame RH (1980) Energy-transducing H+-ATPase of *Escherichia coli*. Reconstitution of proton translocation activity of the intrinsic membrane sector. J Biol Chem 255: 5643–5648.

Nicholls DG, Ferguson SJ (2002) *Bioenergetics*. Academic Press, San Diego, CA.

Nishi T, Forgac M (2002) The vacuolar (H+)-ATPases—nature's most versatile proton pumps. Nat Rev Mol Cell Biol 3: 94–103.

Nishio K, Iwamoto-Kihara A, Yamamoto A, Wada Y, Futai M (2002) Subunit rotation of ATP synthase embedded in membranes: a or beta subunit rotation relative to the c subunit ring. Proc Natl Acad Sci USA 99: 13448–13452.

Nishizaka T, Oiwa K, Noji H, Kimura S, Muneyuki E, Yoshida M, Kinosita K (2004) Chemomechanical coupling in F_1-ATPase revealed by simultaneous observation of nucleotide kinetics and rotation. Nat Struct Mol Biol 11: 142–148.

Noji H, Yasuda R, Yoshida M, Kinosita K (1997) Direct observation of the rotation of F1-ATPase. Nature 386: 299–302.

Noji H, Bald D, Yasuda R, Itoh H, Yoshida M, Kinosita K (2001) Purine but not pyrimidine nucleotides support rotation of F_1-ATPase. J Biol Chem 276: 25480–25486.

Omote H, Sambonmatsu N, Saito K, Sambongi Y, Iwamoto-Kihara A, Yanagida T, Wada Y, Futai M (1999) The gamma-subunit rotation and torque generation in F_1-ATPase from wild-type or uncoupled mutant *Escherichia coli*. Proc Natl Acad Sci USA 96: 7780–7784.

O'Neill J, Roujeinikova A (2008) Cloning, purification and crystallization of MotB, a stator component of the proton-driven bacterial flagellar motor. Acta Cryst F64: 561–563.

Oster G, Wang H (2000) Reverse engineering a protein: the mechanochemistry of ATP synthase. Biochim Biophys Acta 1458: 482–510.

Pänke O, Cherepanov DA, Gumbiowski K, Engelbrecht S, Junge W (2001) Viscoelastic dynamics of actin filaments coupled to rotary F-ATPase: angular torque profile of the enzyme. Biophys J 81:1220–1233.

Park SY, Lowder B, Bilwes AM, Blair DF, Crane BR (2006) Structure of FliM provides insight into assembly of the switch complex in the bacterial flagella motor. Proc Natl Acad Sci USA 103: 11886–11891.

Paster E, Ryu WS (2008) The thermal impulse response of *Escherichia coli*. PNAS 105: 5373–5377.

Pilizota T, Bilyard T, Bai F, Futai M, Hosokawa H, Berry RM (2007) A programmable optical angle clamp for rotary molecular motors. Biophys J 93: 264–275.

Pogoryelov D, Yu J, Meier T, Vonck J, Dimroth P, Muller DJ (2005) The C15 ring of the Spirulina platensis F-ATP synthase: F1/F0 symmetry mismatch is not obligatory. EMBO Rep 6: 1040–1044.

Pogoryelov D, Reichen C, Klyszejko AL, Brunisholz R, Muller DJ, Dimroth P, Meier T (2007) The oligomeric state of C rings from cyanobacterial f-ATP synthases varies from 13 to 15. J Bacteriol 189: 5895–5902.

Powell B, Graham LA, Stevens TH (2000) Molecular characterization of the yeast vacuolar H+-ATPase proton pore. J Biol Chem 275: 23654–23660.

Rao R, Senior AE (1987) The properties of hybrid F1-ATPase enzymes suggest that a cyclical catalytic mechanism involving three catalytic sites occurs. J Biol Chem 262: 17450–17454.

Reid SW, Leake MC, Chandler JH, Lo CJ, Armitage JP, Berry RM (2006) The maximum number of torque-generating units in the flagellar motor of *Escherichia coli* is at least 11. Proc Natl Acad Sci USA 103: 8066–8071.

Rondelez Y, Tresset G, Nakashima T, Kato-Yamada Y, Fujita H, Takeuchi S, Noji H (2005) Highly coupled ATP synthesis by F1-ATPase single molecules. Nature 433: 773–777.

Rubinstein JL, Walker JE, Henderson R (2003) Structure of the mitochondrial ATP synthase by electron cryomicroscopy. EMBO J 22: 6182–6192.

Ryu WS, Berry RM, Berg HC (2000) Torque-generating units of the flagellar motor of *Escherichia coli* have a high duty ratio. Nature 403: 444–447.

Sabbert D, Engelbrecht S, Junge W (1996) Intersubunit rotation in active F-ATPase. Nature 381: 623–625.

Sakaki N, Shimo-Kon R, Adachi K, Itoh H, Furuike S, Muneyuki E, Yoshida M, Kinosita K (2005) One rotary mechanism for F_1-ATPase over ATP concentrations from millimolar down to nanomolar. Biophys J 88: 2047–2056.

Sambongi Y, Iko Y, Tanabe M, Omote H, Iwamoto-Kihara A, Ueda I, Yanagida T, Wada Y, Futai M (1999) Mechanical rotation of the c subunit oligomer in ATP synthase (F0F1): direct observation. Science 286: 1722–1724.

Samuel AD, Berg HC (1995) Fluctuation analysis of rotational speeds of the bacterial flagellar motor. Proc Natl Acad Sci USA 92: 3502–3506.

Samuel AD, Berg HC (1996) Torque-generating units of the bacterial flagellar motor step independently. Biophys J 71: 918–923.

Sato K, Homma M (2000) Multimeric structure of PomA, a component of the Na+-driven polar flagellar motor of *Vibrio alginolyticus*. J Biol Chem 275: 20223–20228.

Schemidt RA, Qu J, Williams JR, Brusilow WS (1998) Effects of carbon source on expression of F0 genes and on the stoichiometry of the c subunit in the F_1F_0 ATPase of *Escherichia coli*. J Bacteriol 180: 3205–3208.

Schneider E, Altendorf K (1982) ATP synthetase (F_1F_0) of *Escherichia coli* K-12. High-yield preparation of functional F0 by hydrophobic affinity chromatography. Eur J Biochem 126: 149–153.

Schwem BE, Fillingame RH (2006) Cross-linking between helices within subunit a of *Escherichia coli* ATP synthase defines the transmembrane packing of a four helix bundle. J Biol Chem 281: 37861–37867.

Seelert H, Poetsch A, Dencher NA, Engel A, Stahlberg H, Müller DJ (2000) Structural biology: proton-powered turbine of a plant motor. Nature 405: 418–419.

Sharp LL, Zhou J, Blair DF (1995a) Features of MotA proton channel structure revealed by tryptophan-scanning mutagenesis. Proc Natl Acad Sci USA 92: 7946–7950.

Sharp LL, Zhou J, Blair DF (1995b) Tryptophan-scanning mutagenesis of MotB, an integral membrane protein essential for flagellar rotation in *Escherichia coli*. Biochemistry 34: 9166–9171.

Shimabukuro K, Yasuda R, Muneyuki E, Hara KY, Kinosita K, Yoshida M (2003) Catalysis and rotation of F1 motor: cleavage of ATP at the catalytic site occurs in 1 ms before 40 degree substep rotation. Proc Natl Acad Sci USA 100: 14731–14736.

Shioi JI, Matsuura S, Imae Y (1980) Quantitative measurements of proton motive force and motility in *Bacillus subtilis*. J Bacteriol 144: 891–897.

Shirakihara Y, Leslie AG, Abrahams JP, Walker JE, Ueda T, Sekimoto Y, Kambara M, Saika K, Kagawa Y, Yoshida M (1997) The crystal structure of the nucleotide-free alpha 3 beta 3 subcomplex of F1-ATPase from the thermophilic *Bacillus* PS3 is a symmetric trimer. Structure 5: 825–836.

Silverman M, Simon M (1974) Flagellar rotation and the mechanism of bacterial motility. Nature 249: 73–74.
Silverman M, Matsumura P, Simon M (1976) The identification of the mot gene product with *Escherichia coli*–lambda hybrids. Proc Natl Acad Sci USA 73: 3126–3130.
Sokolov M, Lu L, Tucker W, Gao F, Gegenheimer PA, Richter ML (1999) The 20 C-terminal amino acid residues of the chloroplast ATP synthase gamma subunit are not essential for activity. J Biol Chem 274: 13824–13829.
Sone N, Hamamoto T, Kagawa Y (1981) pH dependence of H+ conduction through the membrane moiety of the H+-ATPase (F_0xF_1) and effects of tyrosyl residue modification. J Biol Chem 256: 2873–2877.
Sowa Y, Hotta H, Homma M, Ishijima A (2003) Torque–speed relationship of the Na+-driven flagellar motor of *Vibrio alginolyticus*. J Mol Biol 327: 1043–1051.
Sowa Y, Rowe AD, Leake MC, Yakushi T, Homma M, Ishijima A, Berry RM (2005) Direct observation of steps in rotation of the bacterial flagellar motor. Nature 437: 916–919.
Sowa Y and Berry RM (2008) Bacterial flagellar motor. Q Rev Biophys (In press).
Spetzler D, York J, Daniel D, Fromme R, Lowry D, Frasch W (2006) Microsecond time scale rotation measurements of single F_1-ATPase molecules. Biochemistry 45: 3117–3124.
Stahlberg H, Müller DJ, Suda K, Fotiadis D, Engel A, Meier T, Matthey U, Dimroth P (2001) Bacterial Na(+)-ATP synthase has an undecameric rotor. EMBO Rep 2: 229–233.
Stock D, Leslie AG, Walker JE (1999) Molecular architecture of the rotary motor in ATP synthase. Science 286: 1700–1705.
Suzuki H, Yonekura K, Namba K (2004) Structure of the rotor of the bacterial flagellar motor revealed by electron cryomicroscopy and single-particle image analysis. J Mol Biol 337: 105–113.
Tanabe M, Nishio K, Iko Y, Sambongi Y, Iwamoto-Kihara A, Wada Y, Futai M (2001) Rotation of a complex of the gamma subunit and C ring of *Escherichia coli* ATP synthase. The rotor and stator are interchangeable. Biol Chem 276: 15269–15274.
Thomas DR, Morgan DG, DeRosier DJ (1999) Rotational symmetry of the C ring and a mechanism for the flagellar rotary motor. Proc Natl Acad Sci USA 96: 10134–10139.
Thomas DR, Francis NR, Xu C, DeRosier DJ (2006) The three-dimensional structure of the flagellar rotor from a clockwise-locked mutant of *Salmonella enterica serovar Typhimurium*. J Bacteriol 188: 7039–7048.
Turner L, Ryu WS, Berg HC (2000) Real-time imaging of fluorescent flagellar filaments. J Bacteriol 182: 2793–2801.
Ueno T, Oosawa K, Aizawa S (1992) M ring, S ring and proximal rod of the flagellar basal body of *Salmonella typhimurium* are composed of subunits of single protein, FliF. J Mol Biol 227: 672–677.
Ueno T, Oosawa K, Aizawa S (1994) Domain structures of the MS ring component protein (FliF) of the flagellar basal body of *Salmonella typhimurium*. J Mol Biol 236: 546–555.
Wadhams GH, Armitage JP (2004) Making sense of it all: bacterial chemotaxis. Nat Rev Mol Cell Biol 5: 1024–1037.
Wagner R, Apley EC, Hanke W (1989) Single channel H+ currents through reconstituted chloroplast ATP synthase CF_0-CF_1. EMBO J 8: 2827–2834.
Walker JE, Fearnley IM, Gay NJ, Gibson BW, Northrop FD, Powell SJ, Runswick MJ, Saraste M, Tybulewicz VL (1985) Primary structure and subunit stoichiometry of F1-ATPase from bovine mitochondria. J Mol Biol 184: 677–701.
Washizu M, Kurahashi Y, Iochi H, Kurosawa O, Aizawa S, Kudo S, Magariyama Y, Hotani H (1993) Dielectrophoretic measurement of bacterial motor characteristics. IEEE Trans Ind Appl 29: 286–294.
Wilkens S, Zhou J, Nakayama R, Dunn SD, Capaldi RA (2000) Localization of the delta subunit in the *Escherichia coli* F_1F_0-ATPsynthase by immuno electron microscopy: the delta subunit binds on top of the F_1. J Mol Biol 295: 387–391.
Yakushi T, Yang J, Fukuoka H, Homma M, Blair DF (2006) Roles of charged residues of rotor and stator in flagellar rotation: comparative study using H+-driven and Na+-driven motors in *Escherichia coli*. J Bacteriol 188: 1466–1472.
Yamaguchi S, Aizawa S, Kihara M, Isomura M, Jones CJ, Macnab RM (1986a) Genetic evidence for a switching and energy-transducing complex in the flagellar motor of *Salmonella typhimurium*. J Bacteriol 168: 1172–1179.
Yamaguchi S, Fujita H, Ishihara A, Aizawa S, Macnab RM (1986b) Subdivision of flagellar genes of *Salmonella typhimurium* into regions for assembly, rotation and switching. J Bacteriol 166: 187–193.
Yasuda R, Noji H, Kinosita K, Yoshida M (1998) F_1-ATPase is a highly efficient molecular motor that rotates with discrete 120 degree steps. Cell 93: 1117–1124.
Yasuda R, Noji H, Yoshida M, Kinosita K, Itoh H (2001) Resolution of distinct rotational substeps by submillisecond kinetic analysis of F_1-ATPase. Nature 410: 898–904.
Yasuda R, Masaike T, Adachi K, Noji H, Itoh H, Kinosita K (2003) The ATP waiting conformation of rotating F_1-ATPase revealed by single-pair fluorescence resonance energy transfer. Proc Natl Acad Sci USA 100: 9314–9318.

Yorimitsu T, Sowa Y, Ishijima A, Yakushi T, Homma M (2002) The systematic substitutions around the conserved charged residues of the cytoplasmic loop of Na+-driven flagellar motor component PomA. J Mol Biol 320: 403–413.

Yorimitsu T, Mimaki A, Yakushi T, Homma M (2003) The conserved charged residues of the C-terminal region of FliG, a rotor component of the Na+-driven flagellar motor. J Mol Biol 334: 567–583.

Yorimitsu T, Kojima M, Yakushi T, Homma M (2004) Multimeric structure of the PomA/PomB channel complex in the Na+-driven flagellar motor of *Vibrio alginolyticus*. J Biochem 135: 43–51.

York J, Spetzler D, Hornung T, Ishmukhametov R, Martin J, Frasch WD (2007) Abundance of *Escherichia coli* F_1-ATPase molecules observed to rotate via single-molecule microscopy with gold nanorod probes. J Bioenerg Biomemb 39: 435–439.

Yoshida M, Muneyuki E, Hisabori T (2001) ATP synthase–a marvellous rotary engine of the cell. Nat Mol Cell Biol 2:669–677.

Yuan J, Berg HC (2008) Resurrection of the flagellar rotary motor near zero load. Proc Natl Acad Sci USA 105: 1182–1185.

Zhang Y, Wang J, Cui Y, Yue J, Fang X (2005) Rotary torque produced by proton motive force in F_0F_1 motor. Biochem Biophys Res Commun 331: 370–374.

Zhao R, Pathak N, Jaffe H, Reese TS, Khan S (1996) FliN is a major structural protein of the C-ring in the *Salmonella typhimurium* flagellar basal body. J Mol Biol 261: 195–208.

Zhou J, Fazzio RT, Blair DF (1995) Membrane topology of the MotA protein of *Escherichia coli*. J Mol Biol 251: 237–242.

Zhou J, Blair DF (1997) Residues of the cytoplasmic domain of MotA essential for torque generation in the bacterial flagellar motor. J Mol Biol 273: 428–439.

Zhou J, Lloyd SA, Blair DF (1998a) Electrostatic interactions between rotor and stator in the bacterial flagellar motor. Proc Natl Acad Sci USA 95: 6436–6441.

Zhou J, Sharp LL, Tang HL, Lloyd SA, Billings S, Braun TF, Blair DF (1998b) Function of protonatable residues in the flagellar motor of *Escherichia coli*: a critical role for Asp32 of MotB. J Bacteriol 180: 2729–2735.

Zimmermann B, Diez M, Zarrabi N, Gräber P, Börsch M (2005) Movements of the epsilon-subunit during catalysis and activation in single membrane-bound H(+)-ATP synthase. EMBO J 24: 2053–2063.